LA-UR-12-21891
Approved for public release; distribution is unlimited.

Title: Atomistic Simulations of Mass and Thermal Transport in Oxide Nuclear Fuels

Author(s): Andersson, Anders D.
Uberuaga, Blas P.
Du, Shiyu
Liu, Xiang-Yang
Nerikar, Pankaj
Stanek, Christopher R.
Tonks, Michael
Millet, Paul
Biner, Bulent

Intended for: Web

Atomistic Simulations of Mass and Thermal Transport in Oxide Nuclear Fuels

In this talk we discuss simulations of the mass and thermal transport in oxide nuclear fuels. Redistribution of fission gases such as Xe is closely coupled to nuclear fuel performance. Most fission gases have low solubility in the fuel matrix, specifically the insolubility is most pronounced for large fission gas atoms such as Xe, and as a result there is a significant driving force for segregation of gas atoms to grain boundaries or dislocations and subsequently for nucleation of gas bubbles at these sinks. The first step of the fission gas redistribution is diffusion of individual gas atoms through the fuel matrix to existing sinks, which is governed by the activation energy for bulk diffusion. Fission gas bubbles are then formed by either separate nucleation events or by filling voids that were nucleated at a prior stage; in both cases their formation and latter growth is coupled to vacancy dynamics and thus linked to the production of vacancies via irradiation or thermal events.

In order to better understand bulk Xe behavior (diffusion mechanisms) in $UO_{2\pm x}$ we first calculate the relevant activation energies using density functional theory (DFT) techniques. By analyzing a combination of Xe solution thermodynamics, migration barriers and the interaction of dissolved Xe atoms with U, we demonstrate that Xe diffusion predominantly occurs via a vacancy-mediated mechanism, though other alternatives may exist in high irradiation fields. Since Xe transport is closely related to diffusion of U vacancies, we have also studied the activation energy for this process. In order to explain the low value of 2.4 eV found for U migration from independent damage experiments (not thermal equilibrium) the presence of vacancy clusters must be included in the analysis. Next a continuum transport model for Xe and U is formulated based on the diffusion mechanisms established from DFT. After combining this model with descriptions of the interaction between Xe and grain boundaries derived from separate atomistic calculations, we simulate Xe redistribution for a few simple microstructures using finite element methods (FEM), as implemented in the MOOSE framework from Idaho National Laboratory.

Thermal transport together with the power distribution determines the temperature distribution in the fuel rod and it is thus one of the most influential properties on nuclear fuel performance. The fuel thermal conductivity changes as function of time due to microstructure evolution (e.g. fission gas redistribution) and compositional changes. Using molecular dynamics simulations we have studied the impact of different types of grain boundaries and fission gas bubbles on UO_2 thermal conductivity.

Atomistic Simulations of Mass and Thermal Transport in Oxide Nuclear Fuels

David Andersson, Blas Uberuaga, Shiyu Du, Ben Liu, Pankaj Nerikar and Chris Stanek

Los Alamos National Laboratory, Los Alamos, NM

Michael Tonks, Paul Millet and Bulent Biner

Fuel Modeling and Simulation, Idaho National Laboratory, ID

Funding acknowledgement: DOE Nuclear Energy Fuel Cycle Research and Development (FCRD) Campaign, Nuclear Energy Advanced Modeling and Simulation (NEAMS) Program and LANL LDRD.

NEAMS Framework for Multi-Scale Oxide Fuel Modeling

Motivation/Approach – Develop mechanistic materials models with improved accuracy and predictive power using atomic level simulation techniques for application in meso-scale and/or continuum models.

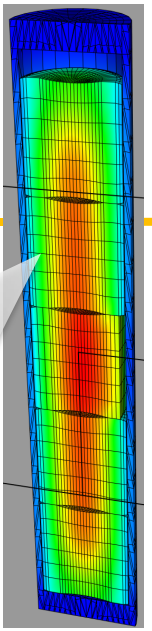

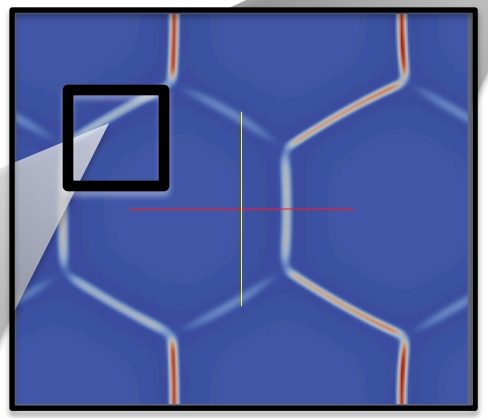

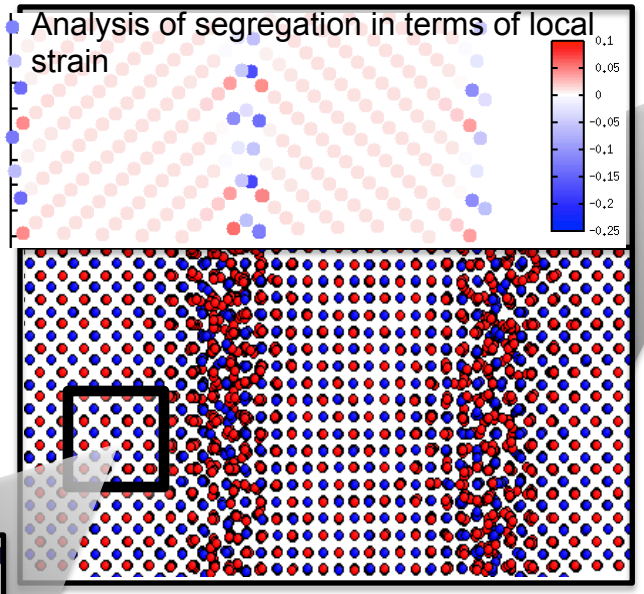

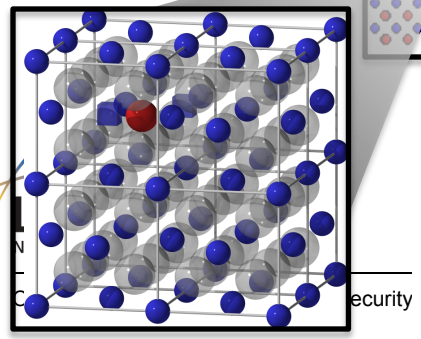

Density Functional Theory

Compositional variations

Bulk diffusion

Bulk thermal conductivity

Molecular Dynamics

Role of idealized grain boundaries in mass and thermal transport.

MARMOT (INL)

Predict and define microstructure state variable evolution

Determine effect of evolution on material properties

BISON-Peregrine (INL)

All results provided to fuel performance codes (MBM).

NNSA

Oxide Fuels Atomistic Scope

Fission gas release

1. Bulk FG and U diffusion as function of composition and stoichiometry.
- FG interaction with microstructure.
- "Upscaling" to meso- and engineering scale.

3. Oxygen transport - upscaling to continuum models.

Thermal conductivity

2. Atomistic simulations of thermal conductivity in UO_2.
- Sensitivity of simulation parameters (size effects).
- Effect of microstructure and fission gas.
- Upscaling of atomistics to meso- and engineering scale (with INL).

Motivation and Objectives

- Formation, redistribution and release of FG are critical determinants of nuclear fuel performance.
- The first controlling step for FG release is diffusion of individual gas atoms to existing gas bubbles or grain boundaries (sinks) governed by the activation energy for bulk diffusion.
- For predictive capabilities need to establish underlying atomistic mechanisms and determine model parameters.
- The next step in the fission gas release process is interactions with microstructure features.

D.R. Olander, "Fundamental Aspects of Nuclear Reactor Fuel Elements" (1976)

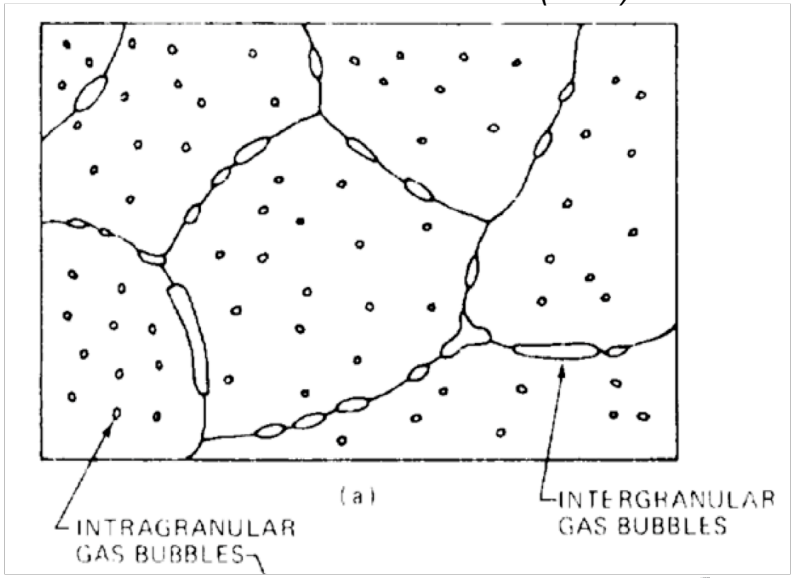

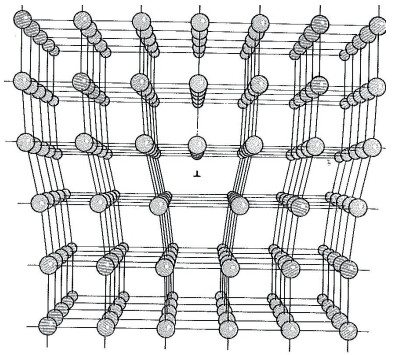

From C.A. Wert and R.M. Thomson "Physics of Solids" (1964).

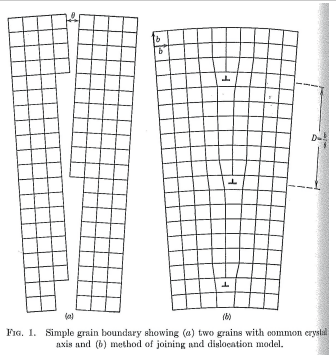

From W.T. Read Jr. and W. Shockley, in F. Seitz "Imperfections in Nearly Perfect Crystals" (1952).

Experimental Activation Energies for U and Xe Diffusion in $UO_{2\pm x}$

Experiments, e.g. Hj. Matzke, *Radiation Effects* **53** (1980) 219.

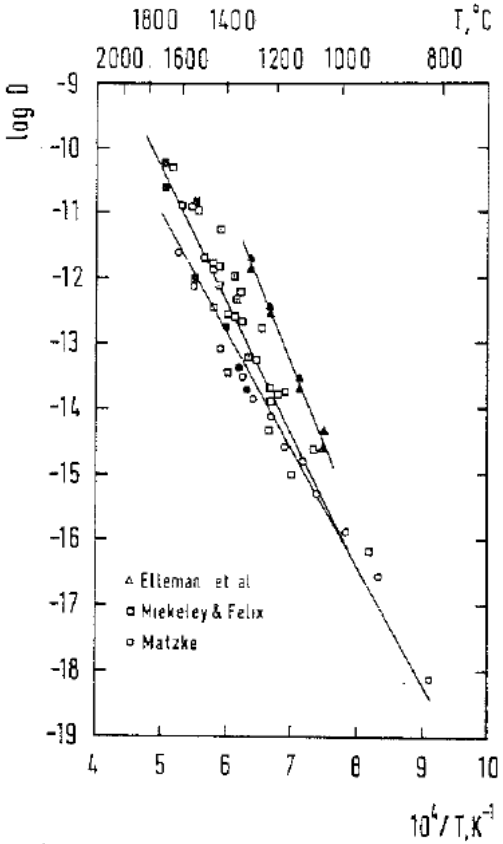

ΔH_A Xe:

ΔH_A=6.0 eV UO_{2-x}.

ΔH_A=3.9 eV UO_2.

ΔH_A=1.7 eV UO_{2+x}.

ΔH_A U:

ΔH_A=7.8 eV UO_{2-x}.

ΔH_A=5.6 eV UO_2.

ΔH_A=2.6 eV UO_{2+x}.

Easier to form U vacancy for x>0 and x=0 than for x<0.

- Effective activation energies determined decades ago, but mechanistic aspects not well understand.

$$D = D_0 \exp\left(-\frac{\Delta H_A}{k_B T}\right)$$

- Required for formulating accurate and predictive diffusion models that account for irradiation.

ED

Methodology

- Density functional theory calculations using VASP.
- Lichtenstein LDA+*U* for U 5f electrons. Literature values for *U* (*U*=4.5 and *J*=0.51 eV). AFM magnetic order is prescribed in all simulations.
- Electronic ground-state determined by occupation matrix control (Dorado *et al.*, PRB 82 035114 (2010), PRB 79 235125 (2009)), reduced symmetries, structural distortions and other methods (e.g., Meredig et al. PRB 82 195128 (2010) and Geng et al. Phys. Rev. B 82, 094106 (2010)).
- 2×2×2 and 2×2×3 fluorite supercell. Ionic relaxations, volume kept fixed.
- MD to find minimum energy structures for complex defects.
- Nudged elastic band (NEB) technique for calculation of migration barriers.
- Charged supercells to model mixed valence character.
- For details see Andersson et al., PRB 84 054105 (2011).

First Principles Calculations of Bulk Xe Diffusion

a) $E = E_F^{V_U}$ b) $E = E_F^{V_U} - E_B$

Xe

c) $E = E_F^{V_U} - E_B$ d) $E = E_F^{V_U} - E_B$

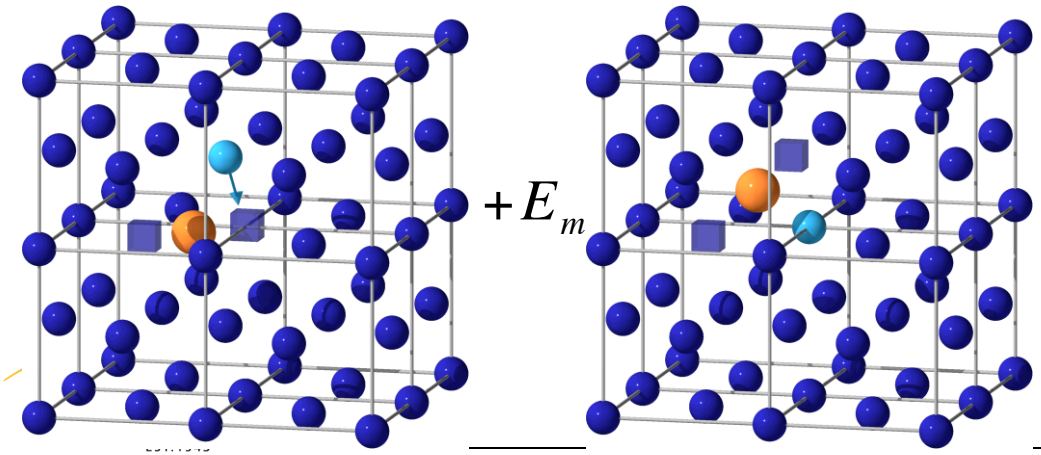

$$\Delta E_a^{Xe} = E_{VU}^{F} - E_B + E_m^{VU,C}(T)$$

Xe atoms occupy different trap sites as function of the $UO_{2\pm x}$ stoichiometry.

Fluorite structure:

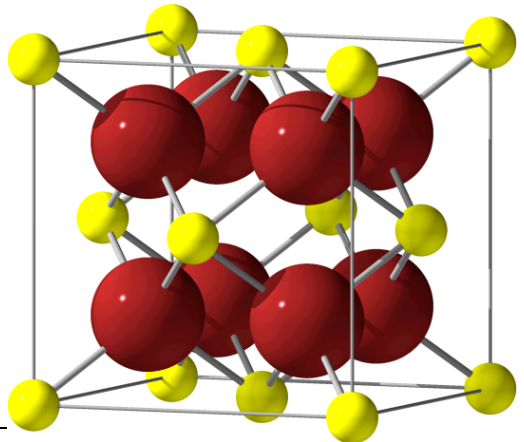

E_m = 3.13/3.73 eV (Xe_{U2})

Bulk U Diffusion Mechanism from DFT

$$\Delta E_a^U = E_{VUOx}^F + E_m^{VUOx}(T)$$

V_U
≈3.53-4.81 eV

V_{UO}
≈3.39-4.07 eV

V_{UO2}
≈3.76-4.51 eV

V_{U2}/V_{U2O}
1.69-2.61 eV/
2.17-2.92 eV

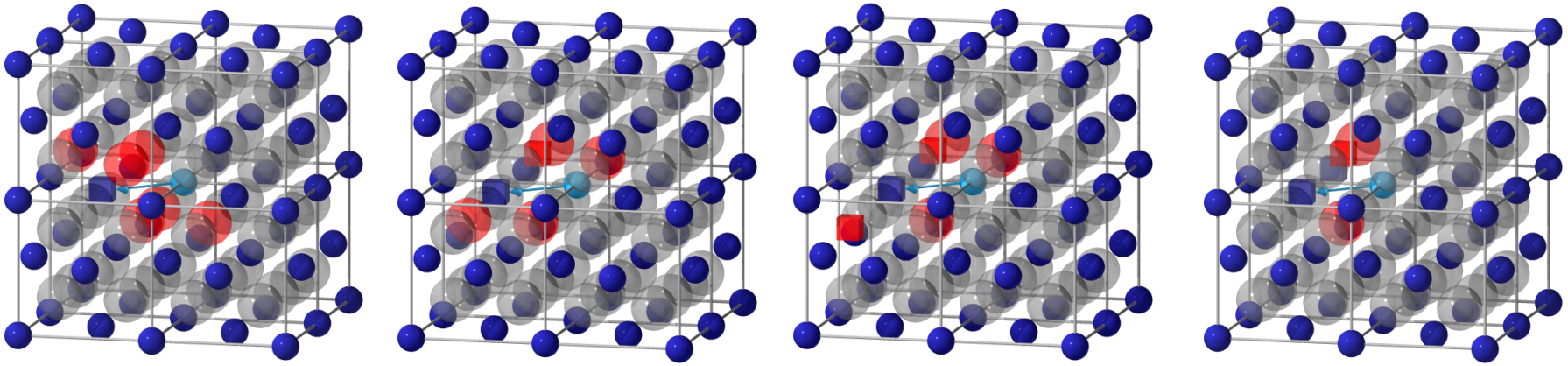

- High barrier is for a_0=5.45 (LDA+U) and low barrier for a_0=5.525 (GGA +U), possibly related to thermal expansion.
- Significant displacement of neighboring O ions for V_U, V_{UO} and V_{UO2}.
- V_U different from exp. barrier (2.4 eV). Explained by V_{U20} or V_{U2} clustering. Experimental barrier obtained for damaged materials.

Calculating the Defect Parameters; Charge Compensation

Simplified thermodynamic defect model due to Catlow[1]

$$E_a^{Xe} = E_{VU}^F - E_B + E_m^{VU,C}(T)$$

	UO_{2-x}	UO_2	UO_{2+x}
V_U	$E_t=E_S$	$E_t=E_S-E_F$	$E_t=E_S-2E_F$
V_{UO}	$E_t=E_S-B_{dv}$	$E_t=E_S-\frac{1}{2}E_F-B_{dv}$	$E_t=E_S-E_F-B_{dv}$
V_{UO_2}	$E_t=E_S-B_{nt}$	$E_t=E_S-B_{nt}$	$E_t=E_S-B_{nt}$

Oxygen Frenkel pair as an example:

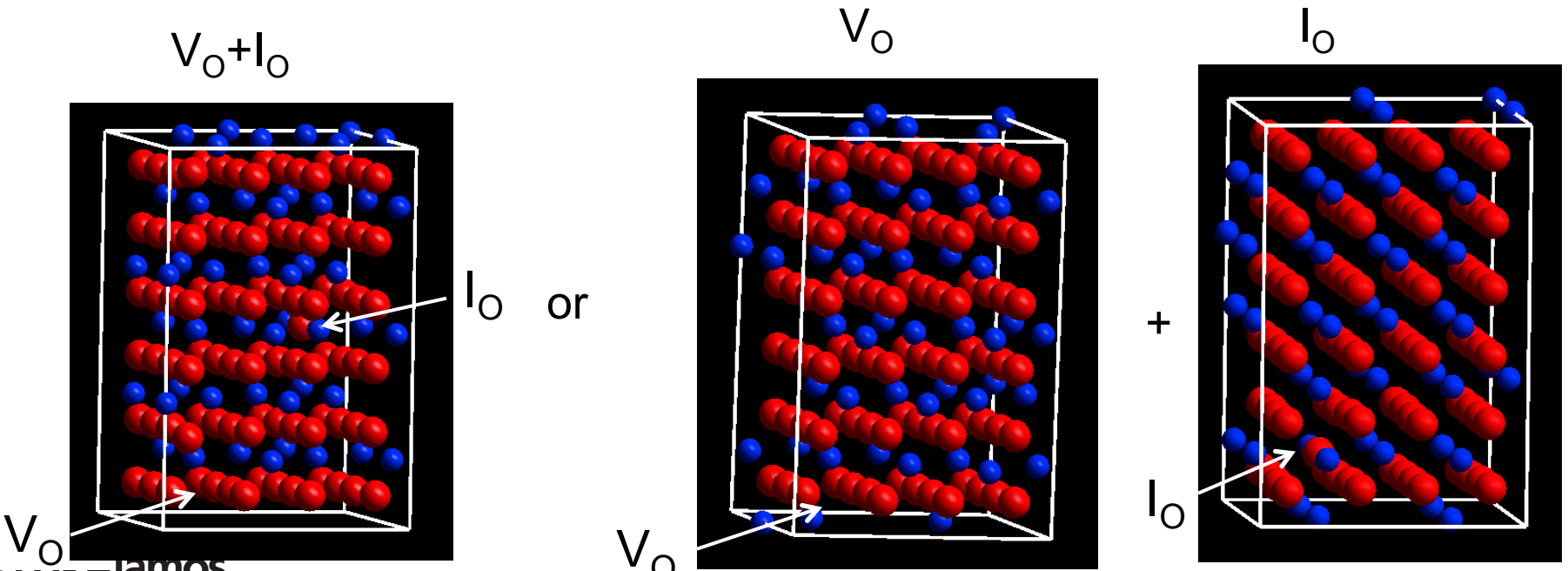

First Principles Calculations of Defect Formation Energies

Simplified thermodynamic defect model due to Catlow[1]

	UO_{2-x}	UO_2	UO_{2+x}
V_U	$E_t=E_S$	$E_t=E_S-E_F$	$E_t=E_S-2E_F$
V_{UO}	$E_t=E_S-B_{dv}$	$E_t=E_S-\frac{1}{2}E_F-B_{dv}$	$E_t=E_S-E_F-B_{dv}$
V_{UO_2}	$E_t=E_S-B_{nt}$	$E_t=E_S-B_{nt}$	$E_t=E_S-B_{nt}$

$$\Delta E_a^{Xe} = E_{VU}^F - E_B + E_m^{VU,C}(T)$$

$$\Delta E_a^U = E_{VUOx}^F + E_m^{VUOx}(T)$$

	E_F (eV)	E_S (eV)	B_{dv}(eV)	B_{nt} (eV)
Neutral	5.26/6.40	10.15/11.96	2.93/3.35	5.58/6.46
Charged	3.32/4.26	6.00/7.65	1.22/1.52	1.43/3.15
One supercell	3.39/4.10	6.39/7.12	1.20/1.33	1.82/1.62
Ref. Exp[1,2]	3.0-4.0	6-7	--	--

"Fluorite"/"J-T"

- Charged supercell calculations include corrections for Coulomb interactions and potential alignments.

Charged or One supercell give best agreement with experiments.

[1] C. R. A. Catlow, Radiat. Eff. Defect. S. 53, 127 (1980).
[2] Hj. Matzke, in Diffusion Processes in Nuclear Materials, ed. R. P. Agarwala, North-Holland, Amsterdam, 1992.

Comparison of First Principles Results to Experimental Values

$$\Delta E_a^{Xe} = E_{VU}^F - E_B + E_m^{VU,C}(T)$$

$$\Delta E_a^U = E_{VUOx}^F + E_m^{VUOx}(T)$$

	Calc.	Exp[1]
$\Delta E_a^U(UO_{2-x})$	7.94-8.69	7.8
$\Delta E_a^U(UO_2)$	6.52-7.20	5.6
$\Delta E_a^U(UO_{2+x})$	2.90-4.18	2.6
$\Delta E_a^{Xe}(UO_{2-x})$	6.52-7.12	6.0
$\Delta E_a^{Xe}(UO_2)$	4.39-4.99	3.9
$\Delta E_a^{Xe}(UO_{2+x})$	1.47-2.07	1.7

	Calc.	Exp. [1]
$E_B(Xe_{UO2})$	2.69 (2.32-3.49)	--
$E_B(Xe_{UO})$	1.43 (1.30-1.95)	--
$E_B(Xe_U)$	1.02 (0.36-1.48)	--
$E_M(V_U)$	3.53-4.81	2.4*
$E_M(V_{UO})$	3.39-4.07	
$E_M(V_{UO2})$	3.76-4.51	--
$E_M(V_{U2})$	1.69-2.61	--
$E_M(V_{U2O})$	2.17-2.92	--
$E_M(Xe_{U2})$	3.13-3.73	3.09/3.14

* “Incorrect” assignment.

[1] Hj. Matzke, in Diffusion Processes in Nuclear Materials, ed. R. P. Agarwala, North-Holland, Amsterdam, 1992.

Thermal equilibrium

Irradiation

Improved Modeling of Uranium Self-Diffusion

- Collaboration between LANL and CEA Cadarache.
- Previous model assumed that experiments were performed at fixed stoichiometry ($UO_{2\pm x}$). Incorrect assumption.
- Experiments: Discrepancies for U activation energies (from 4.4 to 5.6 eV).
- First-principles DFT calculations combined with new thermodynamic model for defect chemistry were used to assess U self-diffusion in nearly stoichiometric UO_2.

Updated thermochemical model

	Calc.	Exp[1]
$\Delta E_a^U(UO_{2-x})$	7.64	7.8
$\Delta E_a^U (UO_2)$	3.97	5.6/4.4
$\Delta E_a^U (UO_{2+x})$	3.19	2.6
$\Delta E_a^{Xe} (UO_{2-x})$	5.61	6.0
$\Delta E_a^{Xe} (UO_2)$	3.94	3.9
$\Delta E_a^{Xe} (UO_{2+x})$	1.79	1.7

$$E_a^{V_U} = 2E_{O_I} + E_S - 2E_{eh} - 2E_{FP_O} + E_{p_{O2}} + E_m^{V_U}$$

- Most favorable mechanism: O-assisted vacancy mechanism with activation energy 4.1-4.9 eV (experimental value: 4.4 eV).
- Similar model should be applied to Matzke's old Xe data.

Interstitial Xe Diffusion in UO_2

Liu et al (*APL*, **98** (2011) 151902)

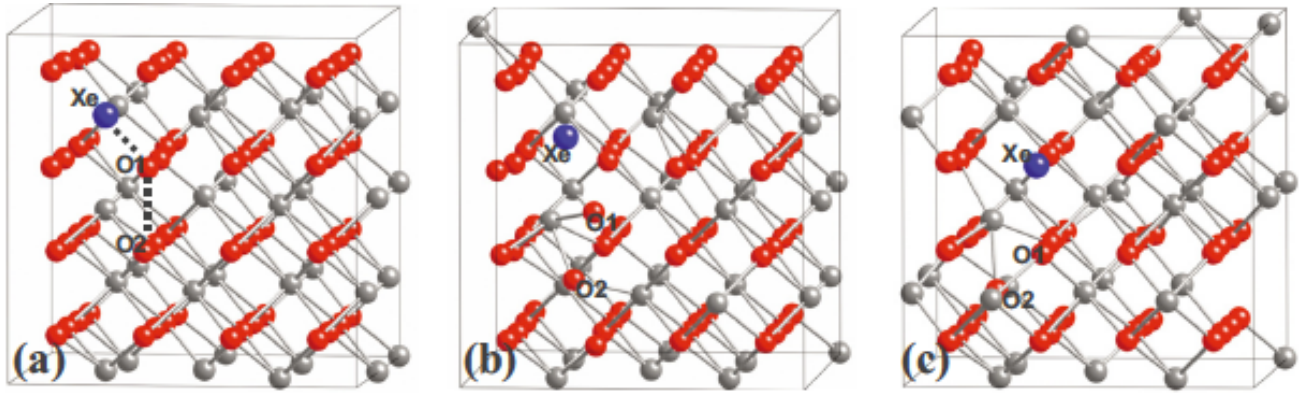

$E_M(Xe_I)$ A	4.48–5.29
$E_M(Xe_I)$ B	1.6-2.41

ΔQ from fuel performance models:

	ΔQ [eV]		ΔQ [eV]
Q1 F&M [2007]	3.09	Q2 F&M Frapcon	1.97
Q2 F&M [2007]	1.19	Q3 F&M Frapcon	0.82
Q1 F&M Frapcon	0.57	ANS5.4	3.14

Bubble Migration Controlled by Surface Diffusion

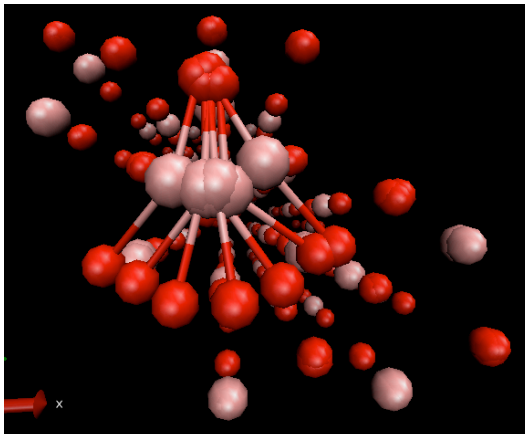

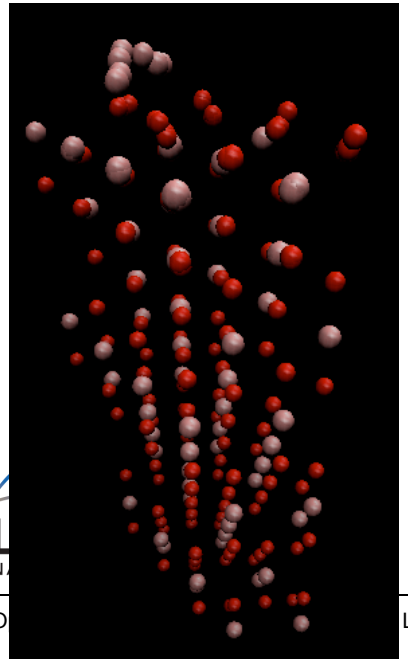

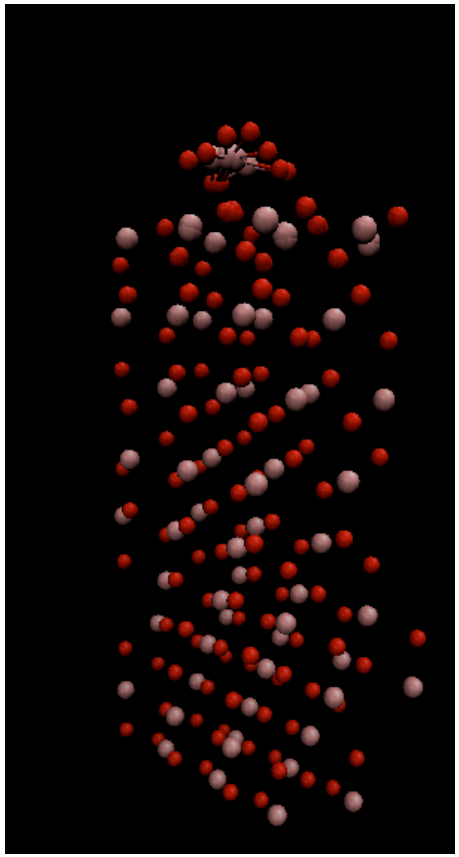

- UO_2 species have a barrier of 1.01 eV on (111) surfaces.
- U atoms have a barrier of 1.26 eV on (111) surfaces.
- Sub-surface U vacancies have a barrier that is about 1 eV lower than bulk barriers.
- Simplified model, does it represent rate limiting step for bubble diffusion?

Xe Segregation to Grain Boundaries

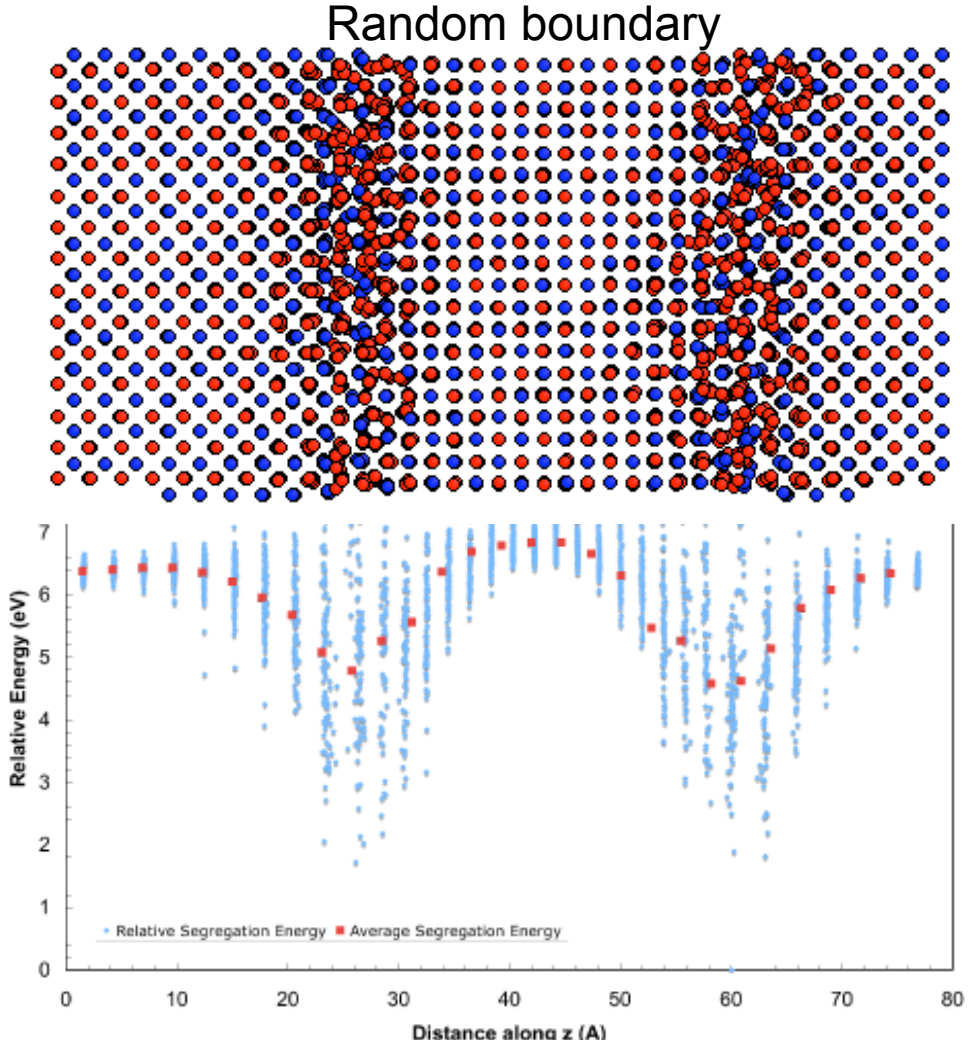

- Lattice statics (Buckingham + Morse)
- Simulations demonstrate that the detailed atomistic structure of grain boundaries impacts fission gas segregation.
- Results at left are for an random boundary – also results for Σ3, Σ5 tilt and Σ5 twist.

"Xenon Segregation to Dislocations and Grain Boundaries," P.V. Nerikar, D. Parftt, D.A. Andersson, S.B. Sinnott, R.W. Grimes, B.P. Uberuaga and C.R. Stanek, PRB 2011.

Coarse Graining Atomistics for Continuum Calculations

Normalized Xe segregation energies from pair potentials to generate fission gas – GB interaction terms as a function of GB structure

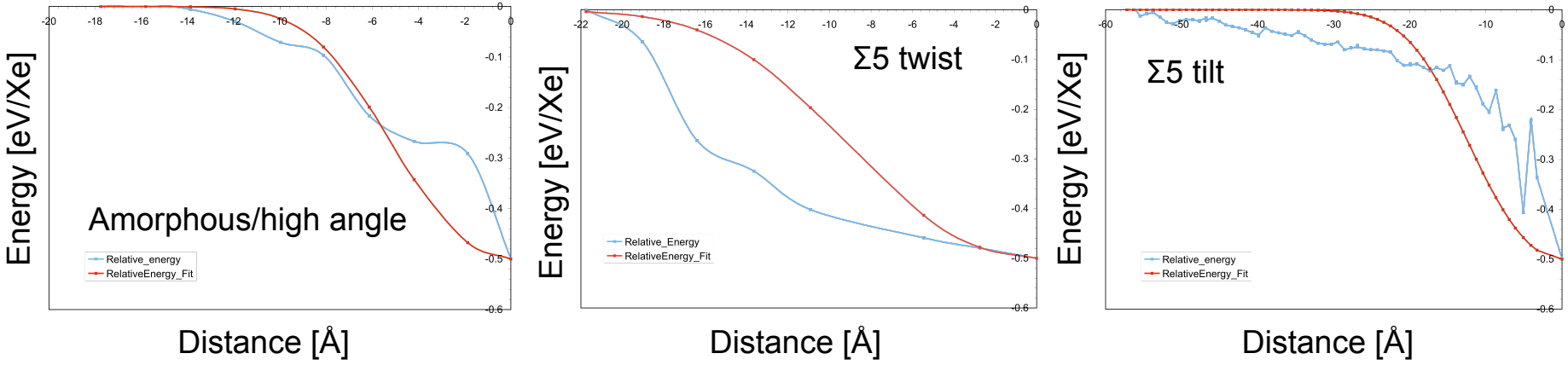

$$f(r) = 1\Big/\left(1+\exp\left(-\left(r-r_0\right)^2/k^2\right)\right)-1 \qquad E_m(r) = 2C_1 f(r)$$

- "Simplistic" approach designed to capture sink strengths and interaction range.

GB type	k (nm)	C_1 (eV)
∑5 Tilt	1.225	4.09
∑5 Twist	0.922	0.97
Amorphous	0.469	6.42

Concentration Dependence of Xe Segregation

Random/high angle

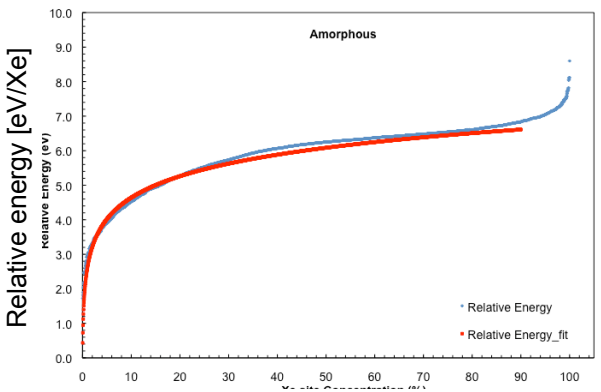

Σ5 tilt

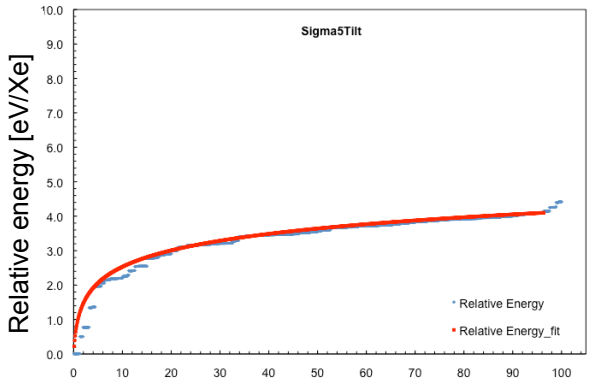

Σ5 twist

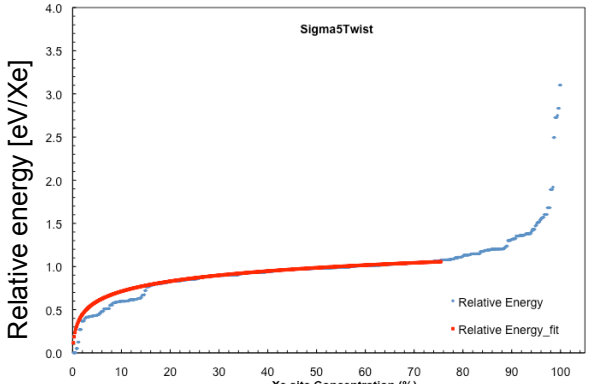

$$g(x) = m\ln\left(x + \exp\left(-b/m\right)\right) + b$$

$$f(r) = 1\Big/\left(1 + \exp\left(-\left(r - r_0\right)^2/k^2\right)\right) - 1$$

$$\frac{E_m^{Xe,gb}\left(y_{Xe}, r\right)}{N_A} = \sum_{i,j}\int_0^{y_{Xe}} 2\left(C_i - g_i\left(y'_{Xe}\right)\right) f_{ij}\left(r_{ij}\right) dy'_{Xe}$$

GB type	m (nm)	b (eV)
∑5 Tilt	0.700	0.900
∑5 Twist	0.171	0.315
Amorphous	0.900	2.562

- Designed to capture sink strengths, interaction range and saturation limits.
- Simplification no “explicit” Xe-Xe interaction (true for both bulk and boundary) and no ΔS from the boundary.

Coarse Graining Atomistics for Continuum Calculations

Thermodynamics (regular solution with parameters from DFT or atomistics):

$$\frac{G_m^{Total}(y_{Xe},y_U,y_{Va})}{N_A} = y_U G_U^{UO_2} + y_{Xe} G_{Xe}^{UO_2} + y_{Va} G_{Va}^{UO_2} + L_{XeVa} y_{Xe} y_{Va} + L_{UVa} y_U y_{Va} + L_{XeU} y_{Xe} y_U +$$

$$+k_B T\left(y_U \ln(y_U) + y_{Xe} \ln(y_{Xe}) + y_{Va} \ln(y_{Va})\right) + \sum_{i,j} \int_0^{y_{Xe}} 2\left(C_i - g_i\left(y'_{Xe}\right)\right) f_{ij}(r_{ij}) dy'_{Xe} +$$

DFT

$$+\sum_{i,j} \int_0^{y_{Xe}} 2\left(C_i^{Va} - g_i^{Va}\left(y'_{Va}\right)\right) f_{ij}^{Va}(r_{ij}) dy'_{Va} + \frac{\varepsilon_{Xe}}{2}(\nabla y_{Xe})^2 + \frac{\varepsilon_U}{2}(\nabla y_U)^2 + \frac{\varepsilon_{Va}}{2}(\nabla y_{Va})^2$$

Potentials

Kinetics (parameters from DFT):

$$M_{Xe} y_{Va} = \frac{D_0}{k_B T}\exp\left(-\frac{\Delta Q}{k_B T}\right) \quad M_{Xe} = \frac{D_0}{k_B T}\exp\left(-\frac{\Delta H_{Xe}}{k_B T}\right) \quad M_U = \frac{D_0}{k_B T}\exp\left(-\frac{\Delta H_U}{k_B T}\right) \quad M_{U_2} = \frac{D_0}{k_B T}\exp\left(-\frac{\Delta H_{U_2}}{k_B T}\right)$$

Transport (clustering + detailed diffusion mechanism):

$$J_{Xe} = -\frac{M_{Xe} y'_{Xe}}{V_m}\nabla\left(\frac{1}{2}\mu_{Xe} + \frac{1}{2}\mu_{Va} - \mu_U\right)$$

$$J_U = -\frac{M_U\left(y_{Va} - y'_{Xe} - y_{Va_2}\right)}{V_m}\nabla\left(\mu_U - \mu_{Va}\right) - \frac{M_{U_2} y_{Va_2}}{V_m}\nabla\left(\mu_U - \mu_{Va}\right) + \frac{2M_{Xe} y'_{Xe}}{V_m}\nabla\left(\frac{1}{2}\mu_{Xe} + \frac{1}{2}\mu_{Va} - \mu_U\right)$$

List of Parameter Values Determined from DFT and Atomistics

Bulk thermodynamic and kinetic parameters for UO_2

U-Xe model		
	Low irr.	High irr.
${}^{o}G_{U}^{UO_2}$ (eV)	0	0
${}^{o}G_{Xe}^{UO_2}$ (eV)	4.35/5.24	4.35/5.24
${}^{0}Ly_{XeU}$ (eV)	10.35	10.35
ΔQ_0 (eV)	4.39	3.13
D_0 (nm/s^2)	$5 \cdot 10^{13}$	$5 \cdot 10^{13}$
U-Xe-Va model	**Low irr.**	**High irr.**
${}^{o}G_{U}^{UO_2}$ (eV)	0	0
${}^{o}G_{Xe}^{UO_2}$ (eV)	4.35/5.24	4.35/5.24
${}^{o}G_{Va}^{UO_2}$ (eV)	2.69/3.39	2.69/3.39
${}^{0}L_{XeVa}$ (eV)	-8.58/-11.7	-16.14/-20.94
${}^{0}L_{UVa}$ (eV)	-0.6/-1.0	4.3/7.1
${}^{0}L_{XeU}$ (eV)	10.35	10.35
ΔH_{Xe} (eV)	3.13	3.13
ΔH_U (eV)	3.94	3.39
ΔH_{U2} (eV)	2.17	2.17
D_0 (nm/s^2)	$5 \cdot 10^{13}$	$5 \cdot 10^{13}$

Segregation parameters for Xe to UO_2 grain boundaries

Grain boundary type	C_i (eV)	k_i (nm)	b_i	m_i
Σ5 tilt	4.09	1.225	0.700	0.900
Σ5 tilt, no electrostatics	3.99	0.387	0.700	0.900
Σ5 twist	0.97	0.922	0.171	0.315
Random	6.42	0.469	0.900	2.562

Defect binding energies controlling cluster equilibriums in UO_2

$$Xe_U + Va_U \Leftrightarrow (Xe_U Va_U) \quad \Delta E_1$$

$$Va_U + Va_U \Leftrightarrow (Va_U Va_U) \quad \Delta E_2$$

	Low irr.	High irr.
ΔE_1	-1.43/-1.95	-2.69/-3.49
ΔE_2	0.10/0.17	-0.72/-1.97

From M. Tonks (INL)

MARMOT *Multiphysics Microstructure Model*

- Predict microstructure evolution due to applied load, temperature gradients and radiation damage.

- **Technique:** Phase field coupled with solid mechanics and heat conduction
- **Solution method**: Implicit finite element using MOOSE framework
- **Goal:** To bring together various mechanisms identified by atomistic simulation to develop multiphysics materials models for fuel performance codes like BISON.

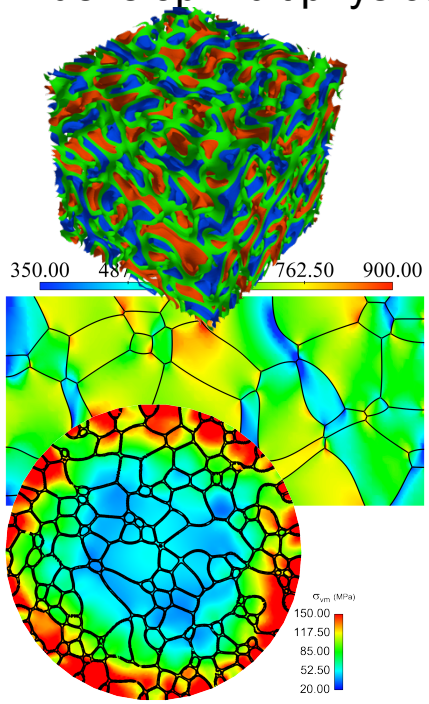

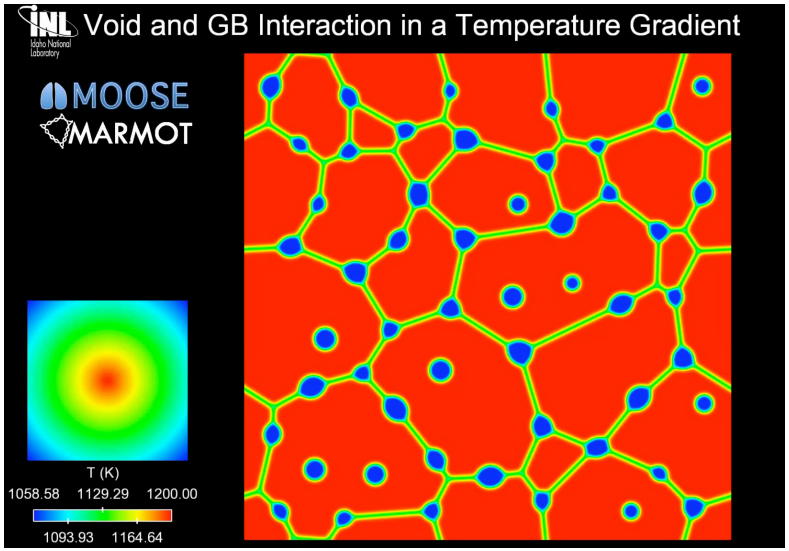

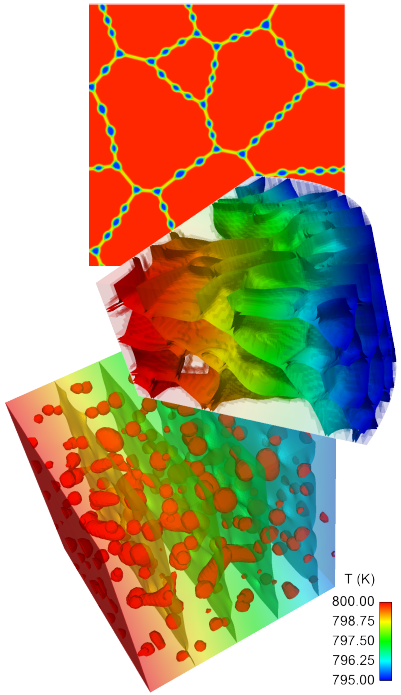

Fission Gas Segregation

- **Stage 1 of fission gas release: Fission gas diffusion to the grain boundaries**

Atomistic

- MD studies determine segregation energies of Xe to various GB

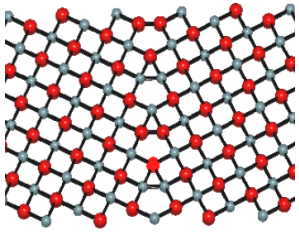

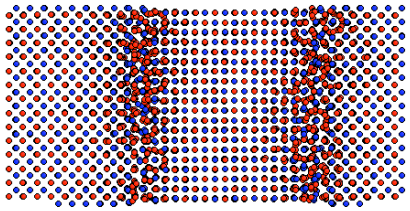

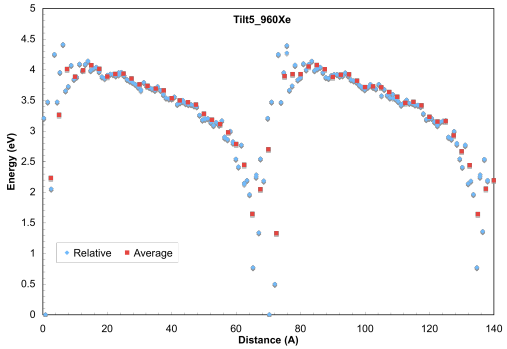

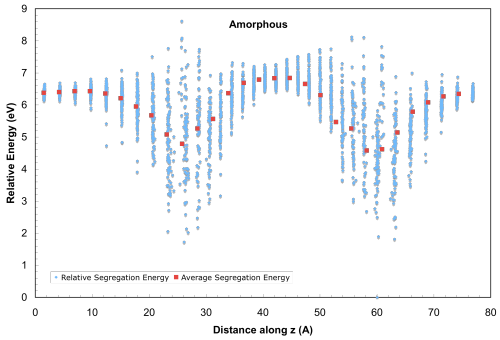

Mesoscale

- MD results used to create a mesoscale segregation model

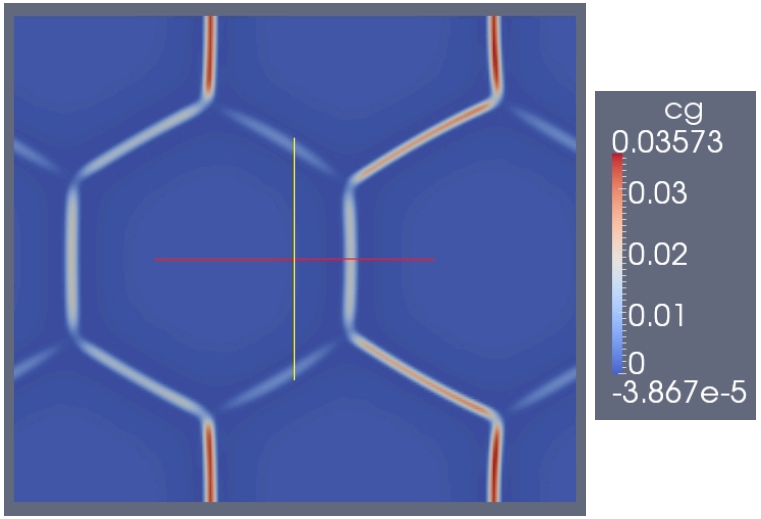

MARMOT for Solving U-Xe-Va Transport Equations

Low irradiation

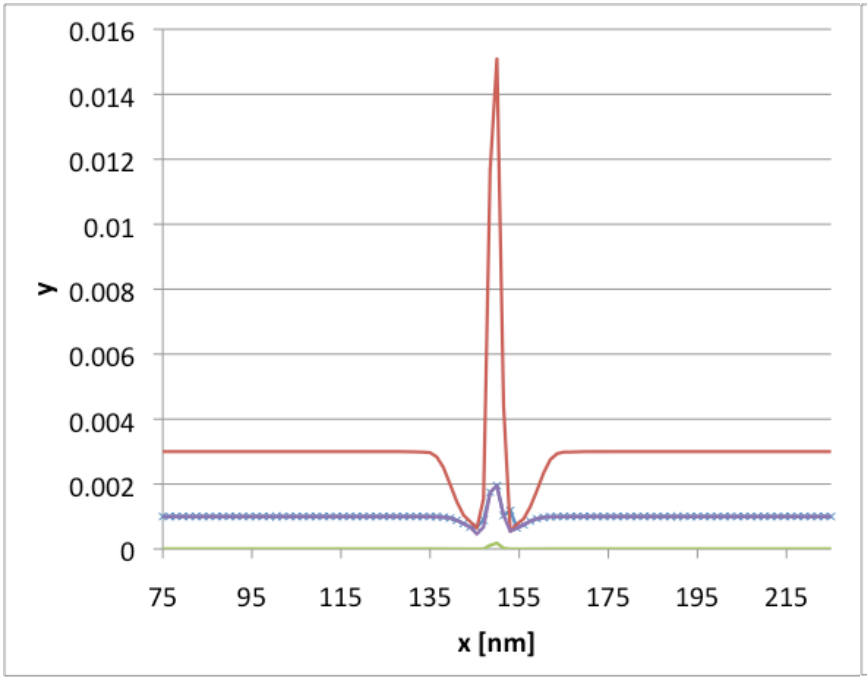

High irradiation

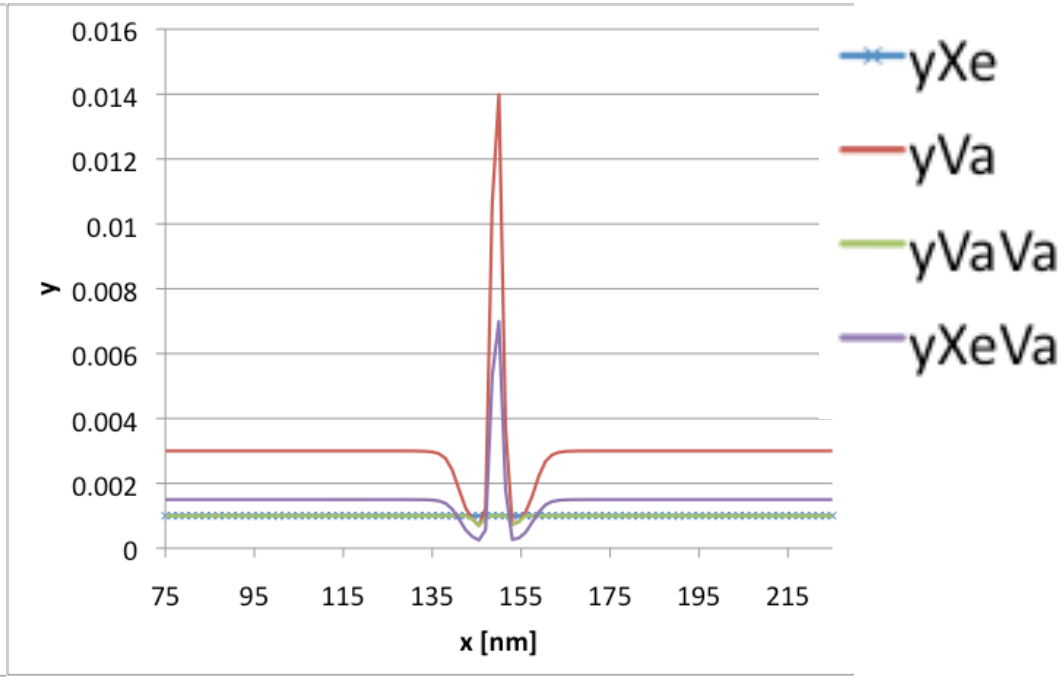

- U-Xe-Va transport equations solved fully coupled using the regular solution model (including clustering).
- Both Xe and vacancies move towards the boundary.
- Under high irradiation vacancies move several orders of magnitude faster than Xe atoms making it difficult to couple time scales.

Atomistic Simulations of UO_2 Thermal Conductivity

$$R_k(T) = d\left(\frac{1}{k(T)} - \frac{1}{k_0^{sc}(T)}\right)$$

(Kapitza Resistance = measure of an interface's resistance to thermal flow)

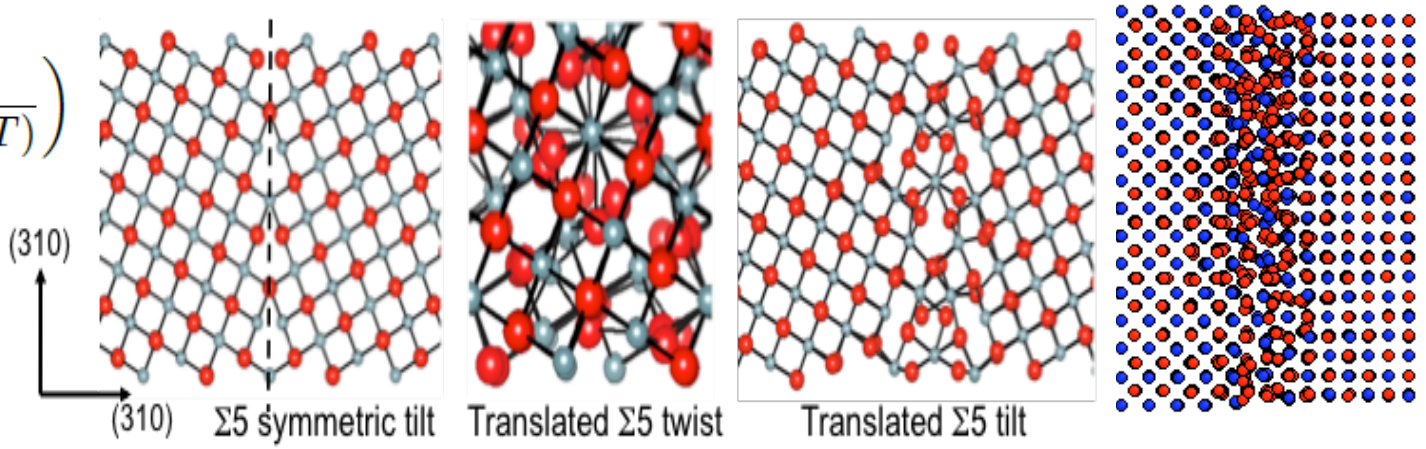

Bulk UO_2

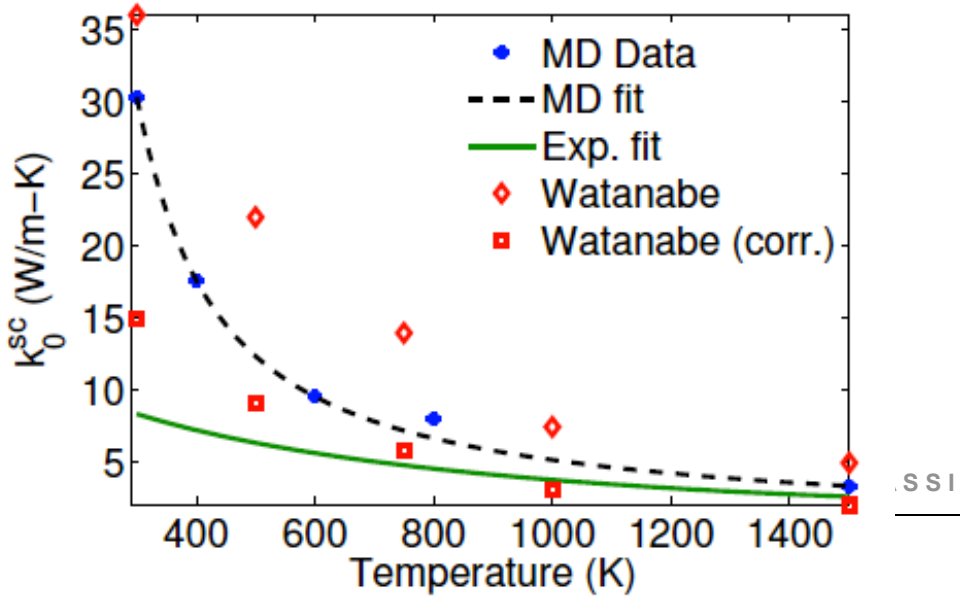

Kapitza resistance

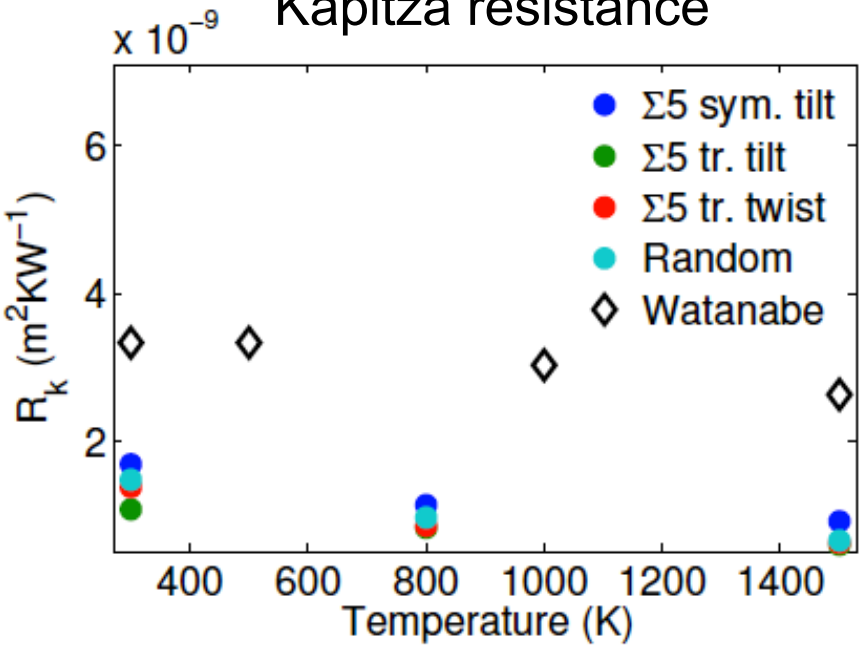

Impact of Xe on Thermal Conductivity

Random Xe atoms

Xe bubble

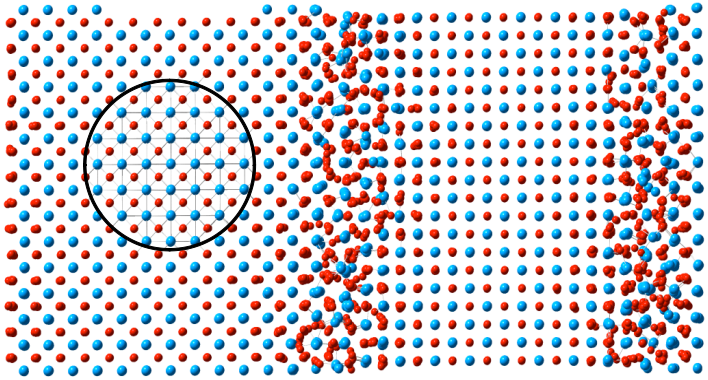

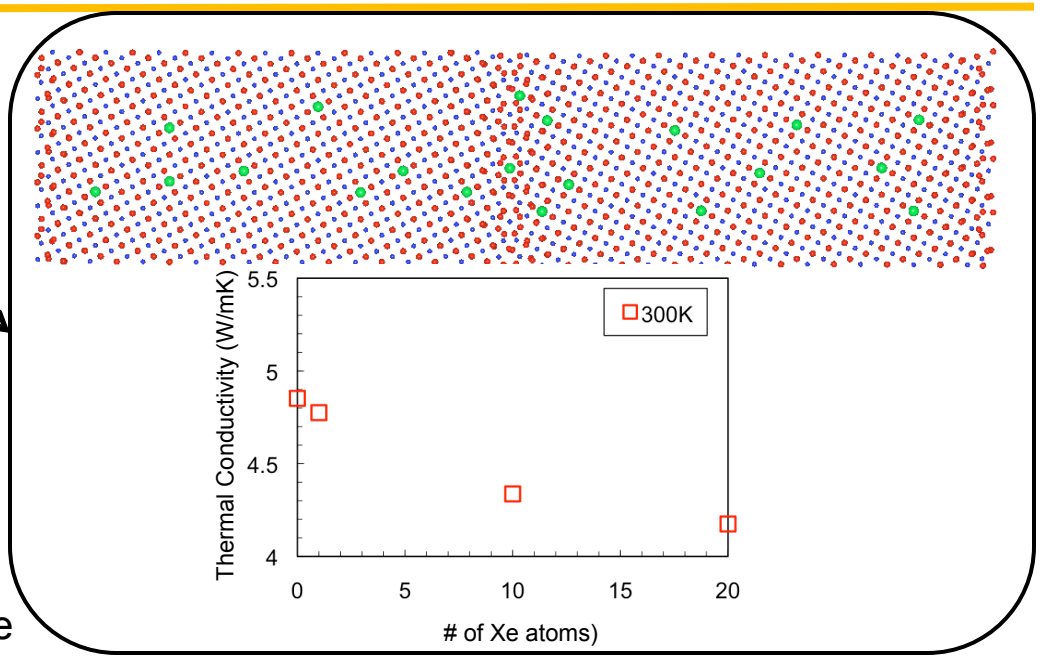

Thermal conductivity as function of microstructure

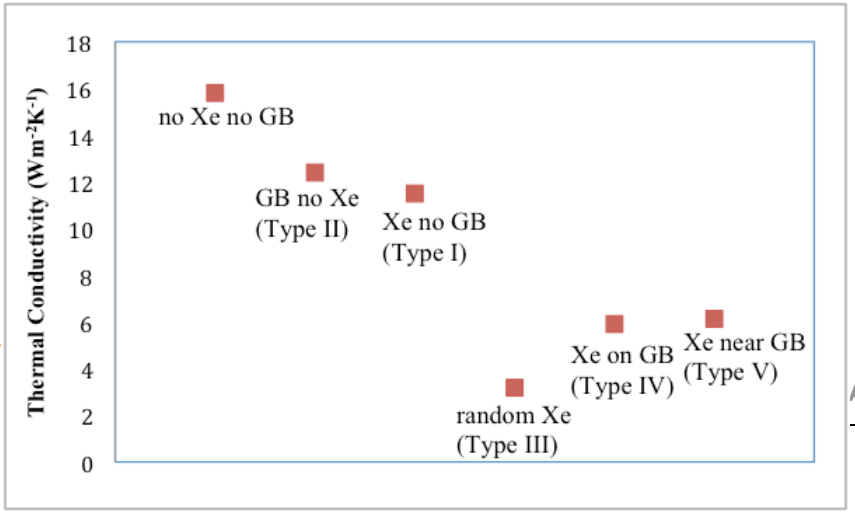

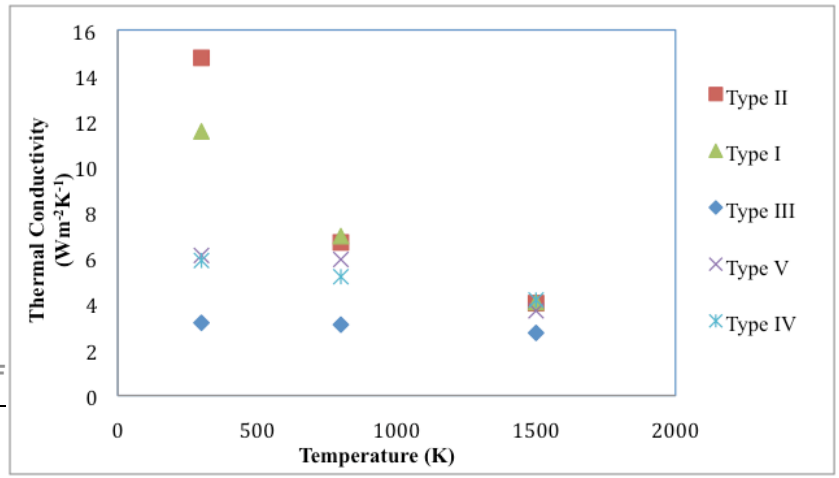

Atomistic-Mesoscale Coupling for Thermal Conductivity

- **Goal: Determine how inter and intragranular fission gas effects the bulk thermal conductivity**

Atomistic

- Single crystal thermal conductivity determined with MD

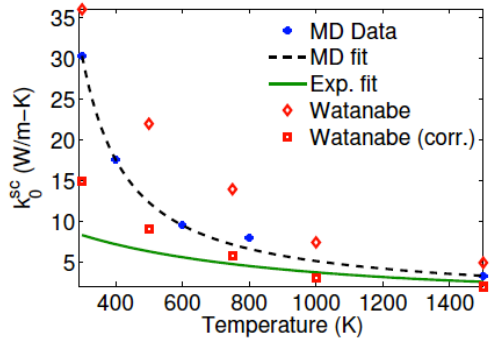

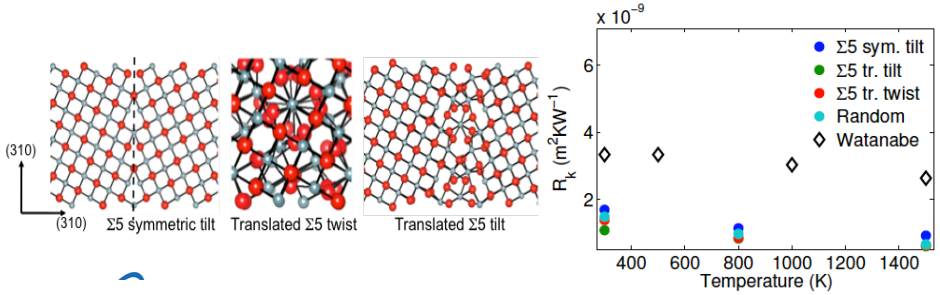

- The UO_2 grain boundary thermal resistance is calculated using MD simulation for three GB types

Mesoscale

Idaho National Laboratory

- Heat conduction simulations investigate the effect of bubbles on thermal conductivity

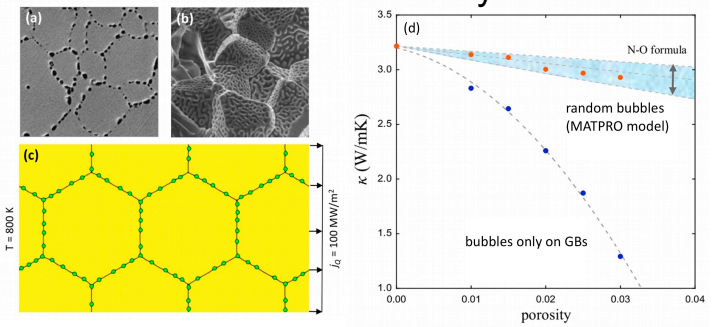

Bubble configuration has a large impact on thermal conductivity: $R'_k = A + (R^0_k - A)(1 - X^C_{GB})$

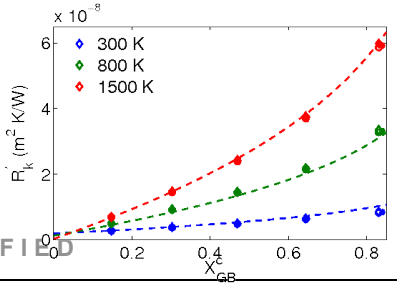

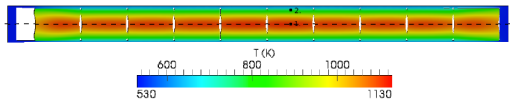

Coupled to Bison fuel performance code.

Atomistic Simulations of UO_2 Oxidation

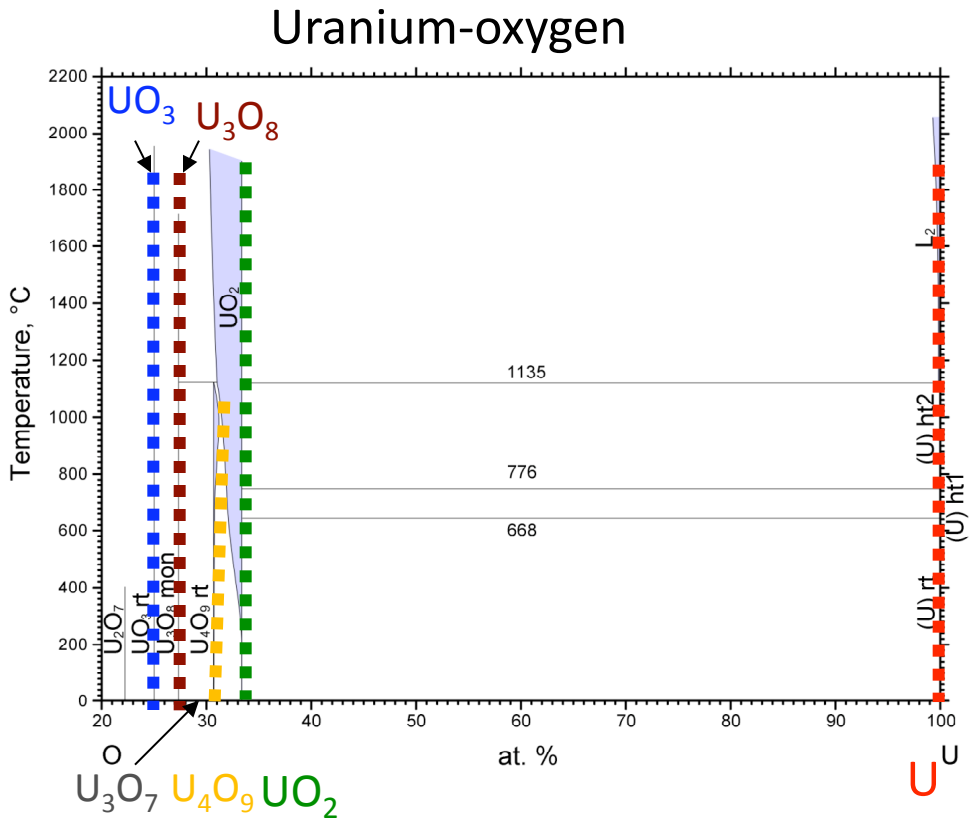

- UO_2, U_4O_9 (p) and U_3O_7 (p) and U_3O_8 (p) are distinct crystallographic phases in UO_{2+x}.
- U_4O_9 and U_3O_7 are derived from the UO_2 fluorite structure, while reconstruction occurs for U_3O_8.
- DFT to investigate thermodynamics and kinetics of Uo2 oxidation and in particular the connection to clustering for UO_{2+x}.

(p) indicates existence of polymorphs.

UO_{2+x} and U_4O_9 structure models

Bevan *et al.*[1] proposed the so-called cubo-octahedron cluster for UO_{2+x} and U_4O_{9-y}.

Cubo-octahedron

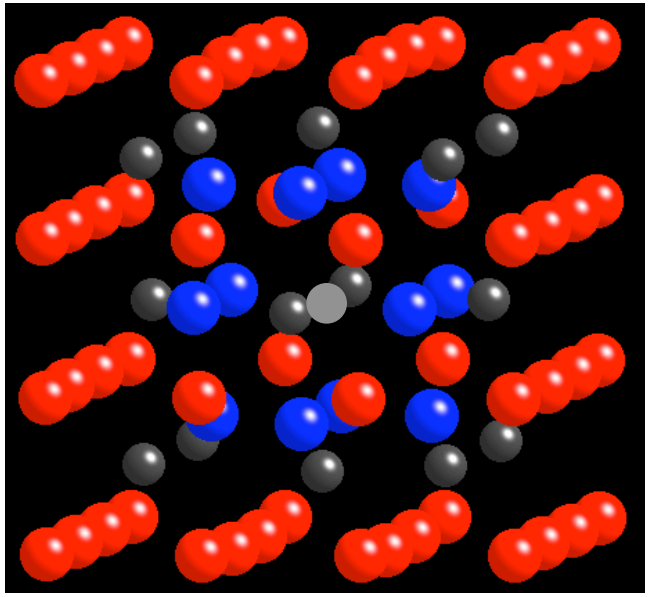

The point defect character in UO_{2+x} was shown to be a function of T and x.

Willis *et al.*[1] found clustering of interstitial-like oxygen ions; introduced to types of interstitial ions, O' and O", to explain neutron diffraction data.

Willis 2:2:2

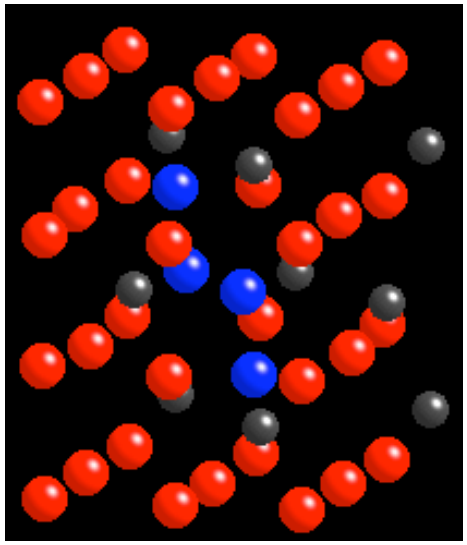

Willis 4:3:2

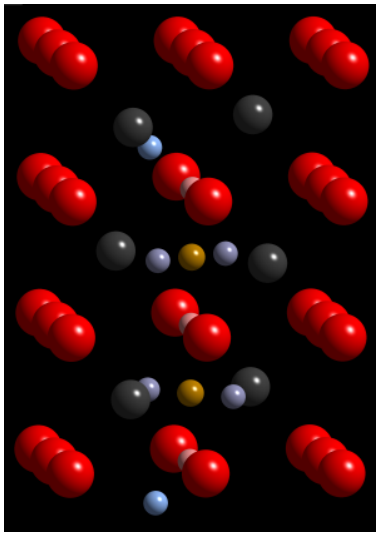

Failed to build U_4O_9 structure model based on the Willis 2:2:2 cluster.

[1] J. Solid State Chem., 61, 1 (1986).

[2] Inorg. Chem. 43, 6922 (2004).

Di-interstitial and Quad-Interstitial Clusters in UO_{2+x} from DFT

- I_2^X is the most stable configuration of di-interstitials, less stable than I_1.
- I_4^X is the most stable state of excess oxygen ions in UO_{2+x}
- Although related, details differ from Willis and cuboctahedral clusters found from neutron diffraction.

Split di-interstitial (I_2^X)

0 eV (r→∞)

$UO_{2.0625}$

+0.16 eV/O ($2I_1$)

+0.19 eV/O (I_2^X)

+0.32 eV/O (I_2^0)

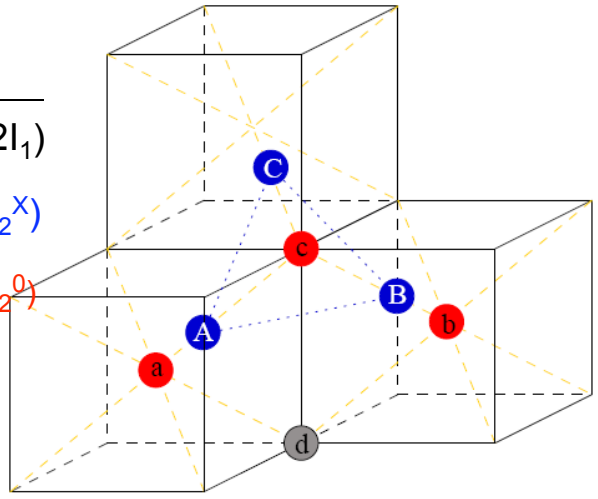

The split di-interstitial (blue) is formed from two NN octahedral interstitials that dislocate a regular oxygen ion (red).

Split quad-interstitial (I_4^X)

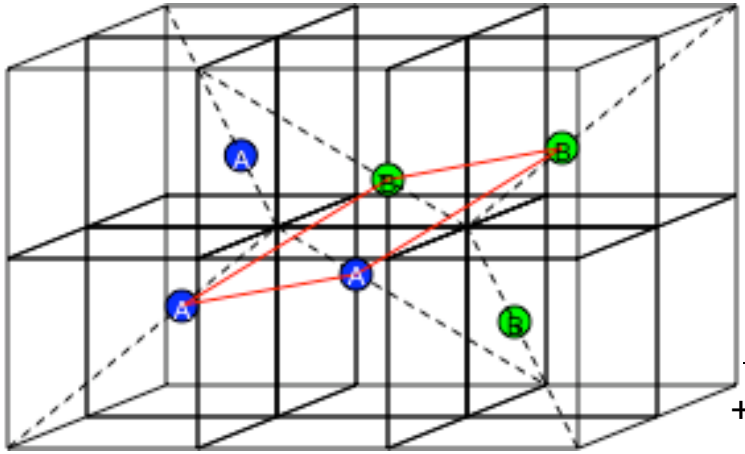

0 eV (r→∞)

$UO_{2.125}$

+0.21 eV/O ($4I_1$)

-0.18 eV/O (I_4)

+0.04 eV/O (I_5)

Two split di-interstitials (blue and green) make up a stable cluster in AnO_{2+x}.

Configurational Stability of Large O Clusters

- Ab Initio MD simulations at T=500 K and T=1000 K.
- The I_5^C cluster transforms into “1.5” interconnected I_4^X clusters with a barrier of 0.1-0.3 eV. The new I_5 cluster is 0.4-0.6 eV more stable than I_5^C.
- Simulations show that the detailed ordering of I_O for I_5 clusters are closely coupled to the distribution of U^{5+} ions. I_O transformations also involve hopping of U^{5+}.
- Raises interesting and largely unexplored questions regarding finite temperature properties coupled to the partial and complete disordering U^{5+}.

I_4^X relaxed (-2.60 eV/O)

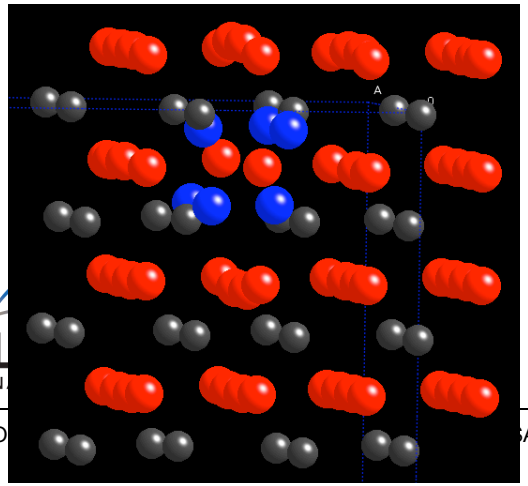

I_5^C relaxed (-2.46 eV/O)

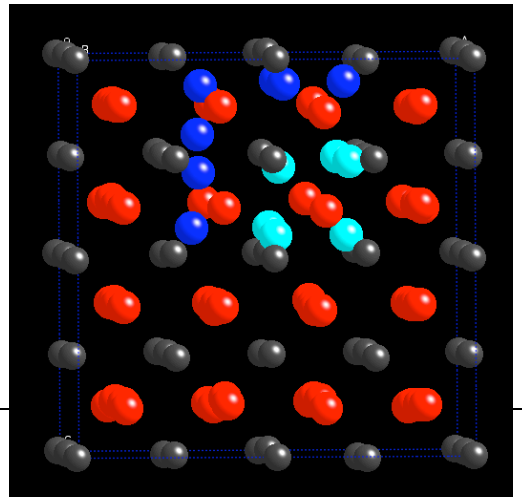

Equil. I_5 (-2.55 eV/O)

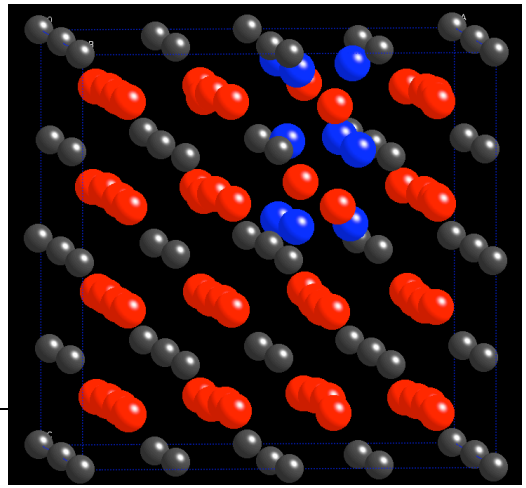

Ordering of Defect Clusters in U_4O_9

U_4O_9(111) [0.52 eV]

Split di-interstitials in {111} planes

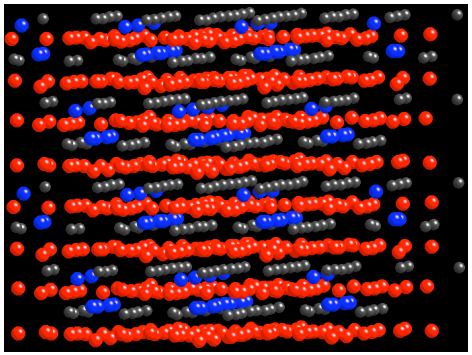

U_4O_9(1-10) [0.38 eV]

Split di-interstitials (transformed byrelax) along (1-10)

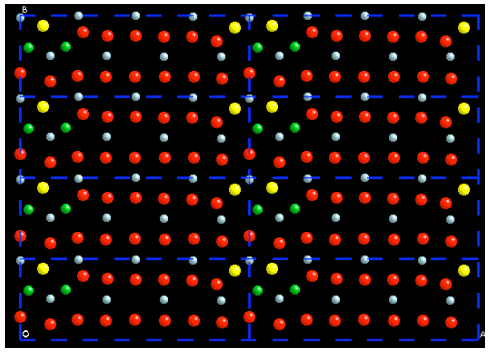

U_4O_9(Oct.) [0.77 eV]

O ions in the octahedral interstitial position

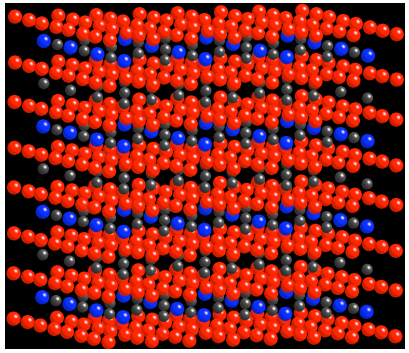

U_4O_9(bcc)/ U_4O_9(bccr) [0/0.01 eV]Ordered arrangement of split quad-interstitials

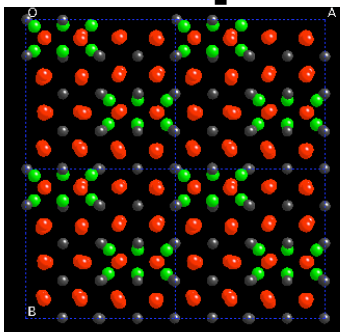

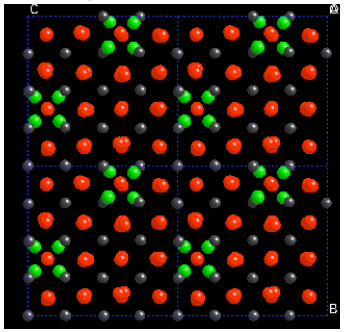

In fact U_4O_{9-y} is more stable and the predicted two phase-field involves UO_2-U_4O_{9-y} in accordance with exp. phase diagram.

Calculations also indicate that U_4O_9(bcc) is more stable than the ordered arrangements of cubo-octahedrons (without central oxygen ion).

U_4O_9 Structures Described as Ordering of Split Di-Interstitials in {111} Planes

(a) UO_2

-U-O-O-U-O-O-U-O-O-U-O-O-

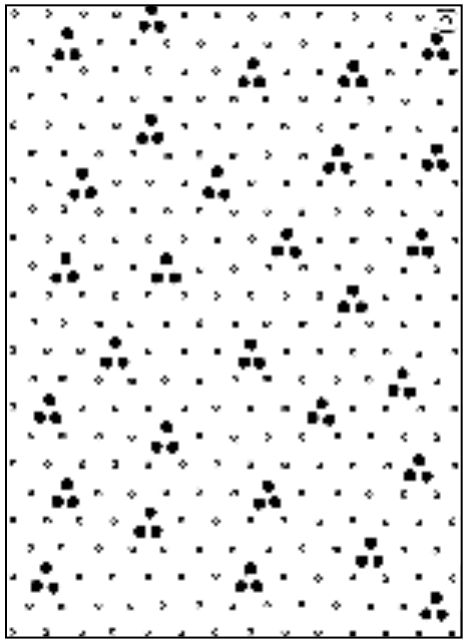

Experimental (111) surface

(b) U_4O_9(111)

-U-O-O-U-O-O-U-O-O-U-O-O-

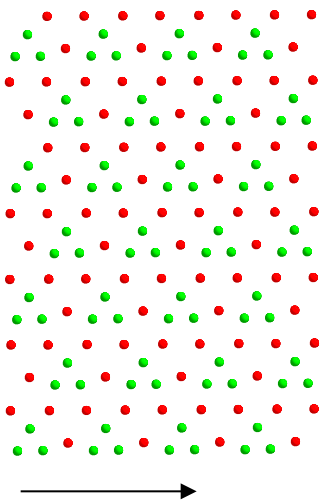

<1-10>

U_4O_9(111) [0.52 eV]
Split di-interstitials in {111} planes

(c) U_4O_9(1-10)

-U-O-O-U-O-O-U-O-O-U-O-O-

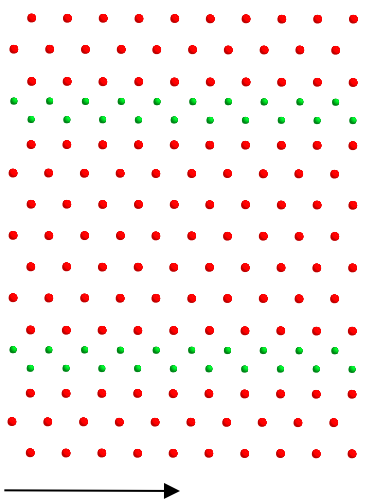

<1-10>

U_4O_9(1-10) [0.38 eV]
Split di-interstitials along (1-10)

(d) U_4O_9(bcc)

-U-O-O-U-O-O-U-O-O-U-O-O-

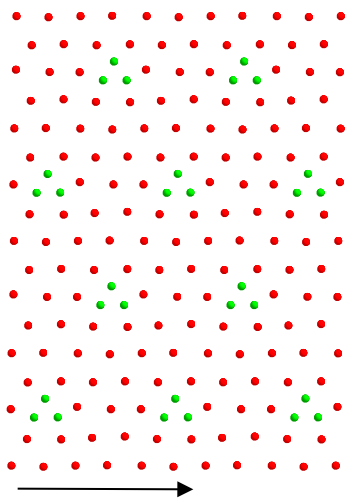

<1-10>

U_4O_9(bcc) [0 eV]
Ordering of split quad-interstitials

- The split di-interstitial is the fundamental building block of O clusters.
- Driving force to distribute the split di-interstitials between different planes (b → c) as well as separate them from each other within each plane (c → d).

Comparison to Neutron PDF data

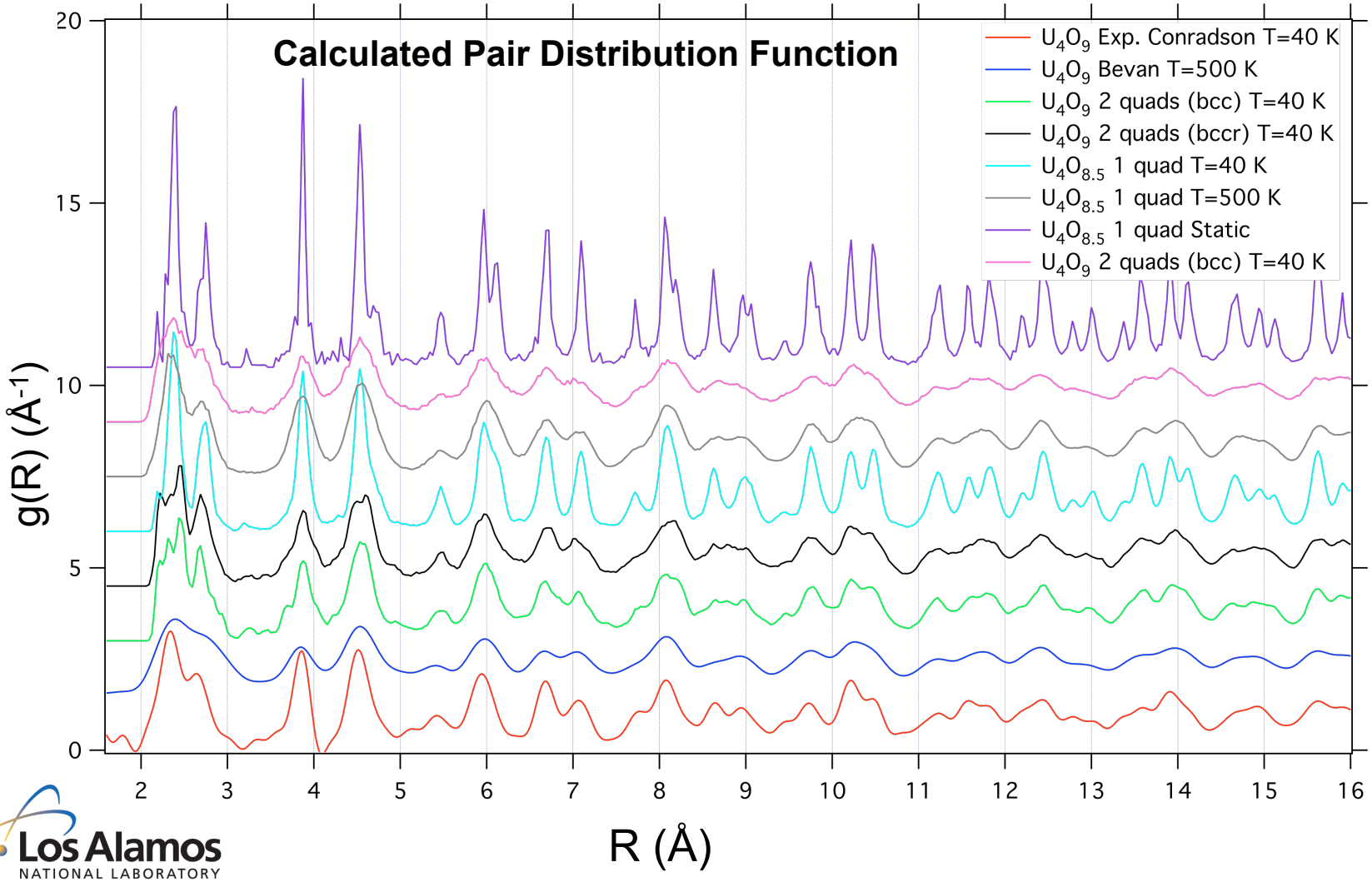

Beyond U_4O_9 (x>0.25 in UO_{2+x}): U_3O_7 and U_3O_8

- Many experimental studies with details that cannot be addressed here: G. C. Allen and P. A. Tempest, Proc. R. Soc. Lond. A **406**, 325 (1986), L. Desgranges et al., Inorg. Chem. **48**, 7585–7592 (2009), G. Rousseau et al., J. Nucl. Mater. **355**, 10 (2006), Allen and Holmes, J. Nucl. Mater. **223,** 231 (1995), F. Garrido *et al.*, J. Nucl. Mater. **322,** 87 (2003), etc.
- Neutron diffraction data describes U_3O_7 as an ordering of (distorted) cuboctahedrons.

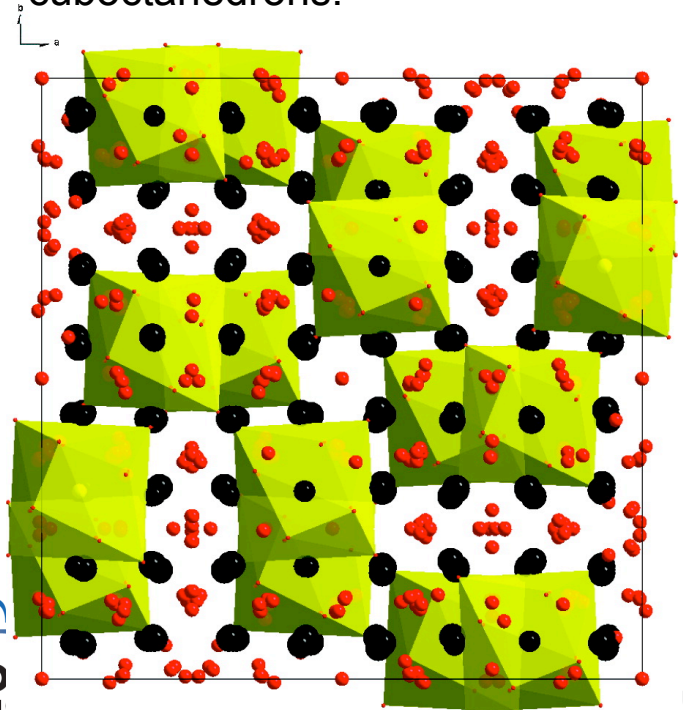

From Desgranges *et al.*, Inorg. Chem. **48**, 7585 (2009).

- U_3O_8 is expanded along the [111] lattice vector and the O ions are re-arranged compared to UO_2, however the cation sublattice in (111) planes still match the (111) fluorite lattice. Originally from Allen and Holmes.

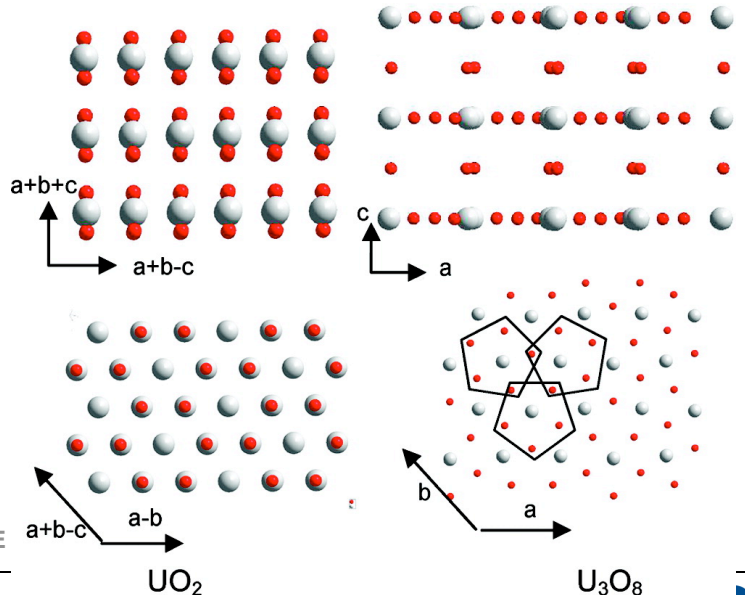

From Desgranges *et al.*, Inorg. Chem. **48**, 7585 (2009).

UO_{2+x} (x>0.25) 2×2×2 Supercell with Multiple I_4, MD at 1200-1500 K (Annealing)

3 I_4^X: $UO_{2.375}/U_3O_{7.05}$ O, O, U

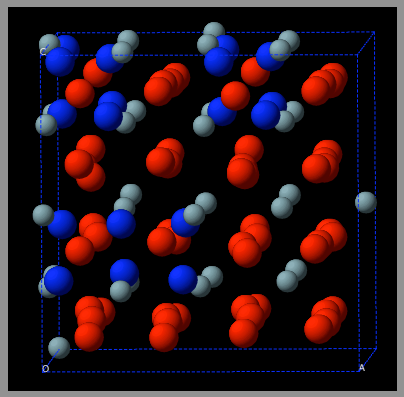

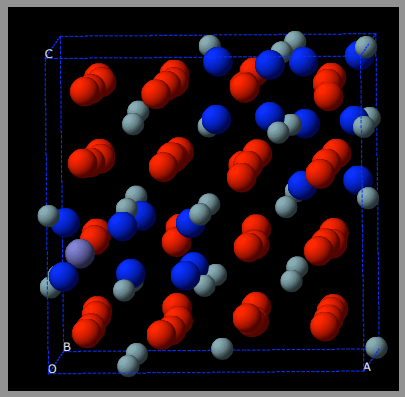

-2.28 eV/O ⇨ -2.38 eV/O

4 I_4^X: $UO_{2.5}/U_3O_{7.5}$

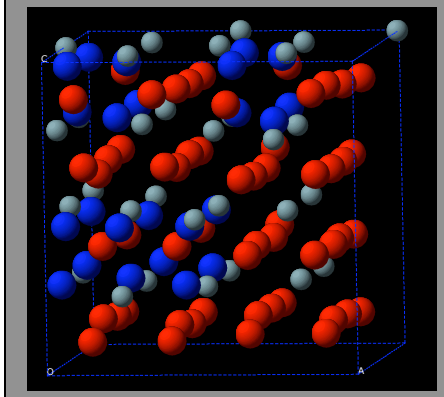

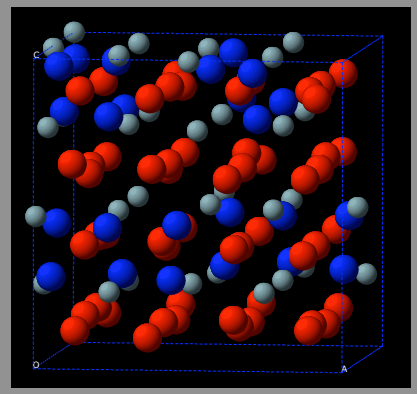

-2.00 eV/O ⇨ -2.25 eV/O

$UO_{2.3125}/U_3O_{6.9375}$

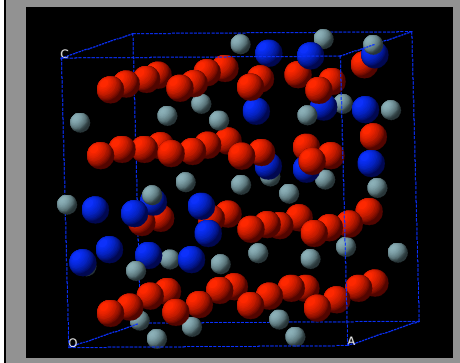

-2.51 eV/O

$UO_{2.125}$ (I_4^X)

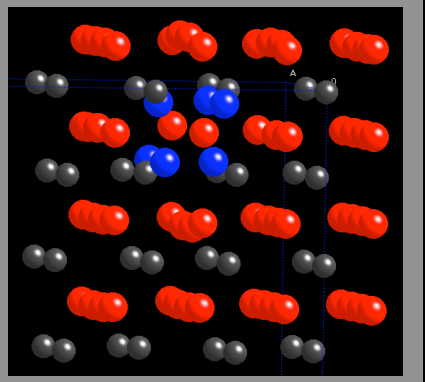

-2.69 eV/O

$UO_{2.625}/U_3O_{7.875}$

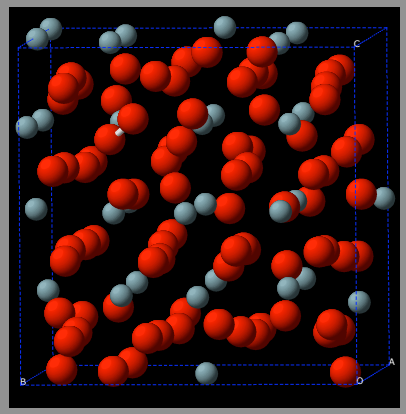

-2.00 eV/O

$UO_{2.75}/U_3O_{8.25}$

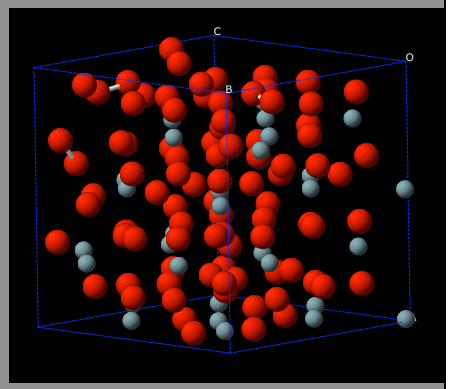

-1.48 eV/O

U_3O_{8-y} Relaxations

2×1×3 U_3O_8 supercell allows for transformation to the fcc ABC stacking on the cation sublattice.

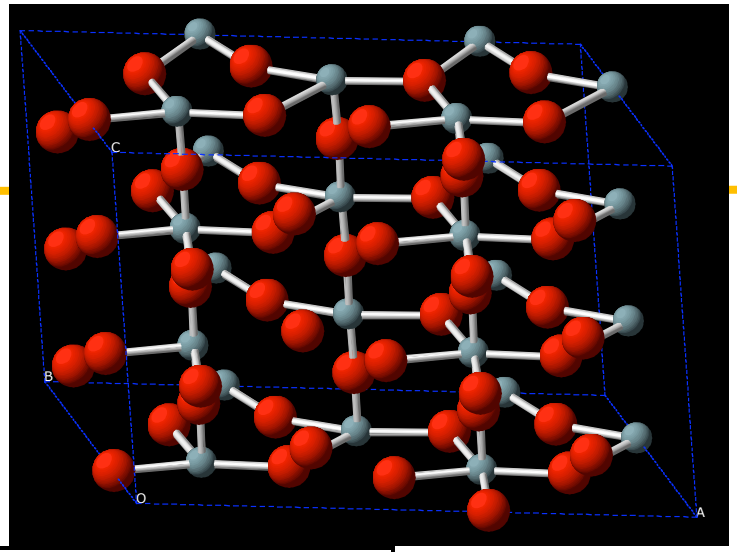

$UO_{2.222}/U_3O_{6.66}$

[111] contraction: -2.49 eV/O

No [111] contraction: 1.98 eV/O

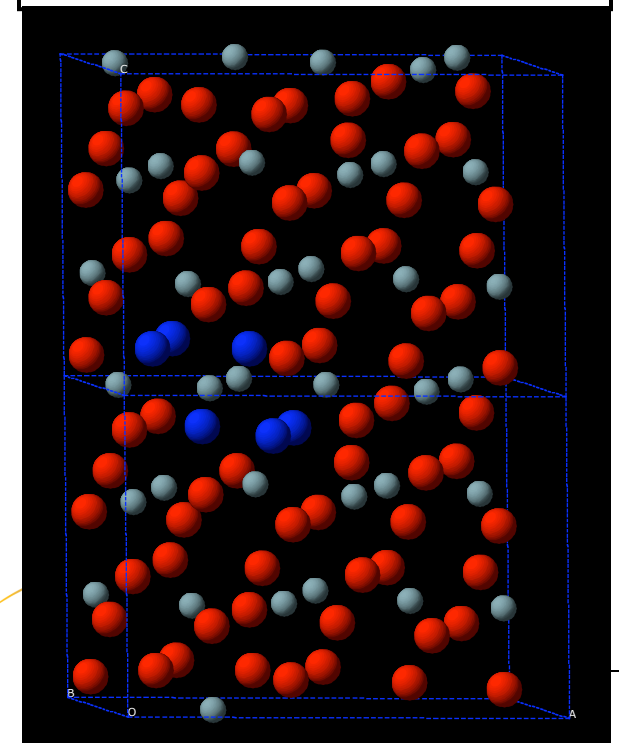

O

O

U

$UO_{2.433}/U_3O_{7.3}$

[111] contraction: -2.66 eV/O

No [111] contraction: -1.62 eV/O

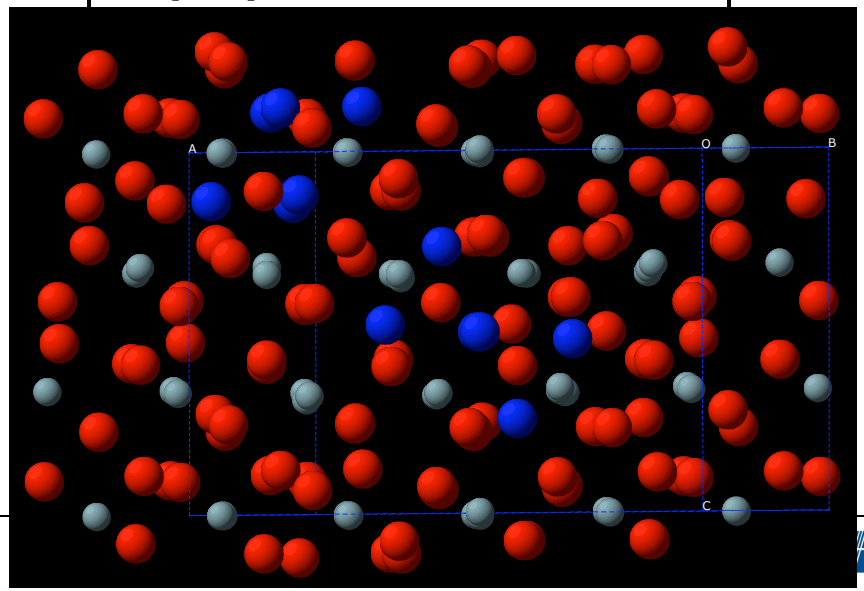

Currently studying U_3O_7 within 2×2×3 U_3O_8 supercell

New Model for Low Temperature Phase of U_4O_{9-y} Derived from DFT

U_4O_{9-y}

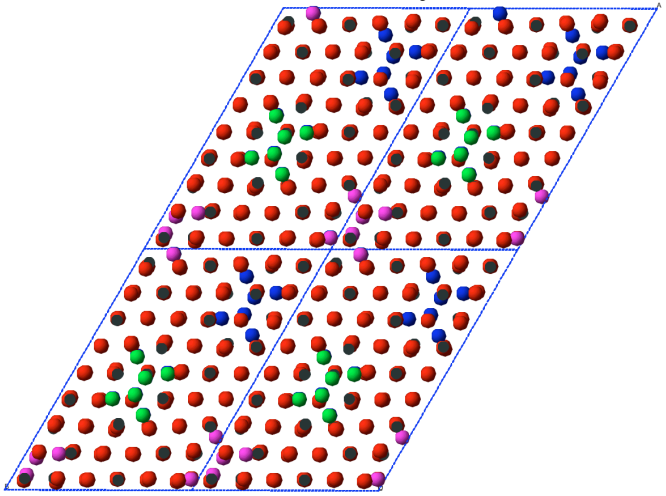

UO_2

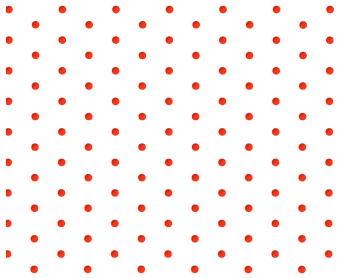

Ordering of oxygen clusters on {111} planes in U_4O_{9-y}

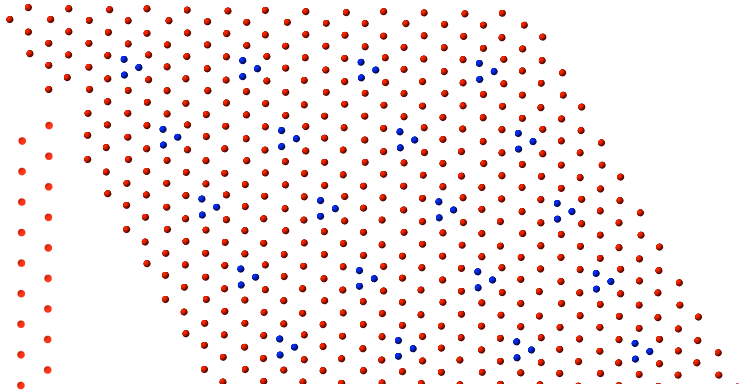

- Strong driving force for O ions to cluster. Repulsion between clusters leads to separation of individual cluster units on {111} planes.
- Optimal packing yields y=0.074, close to exp. value of y=0.06. Above structure deviates slightly from optimal packing (too large unit cell for DFT).
- Disordering of clusters and U^{5+} ions at finite T lead to polymorphs.

Neutron diffraction vs. theory

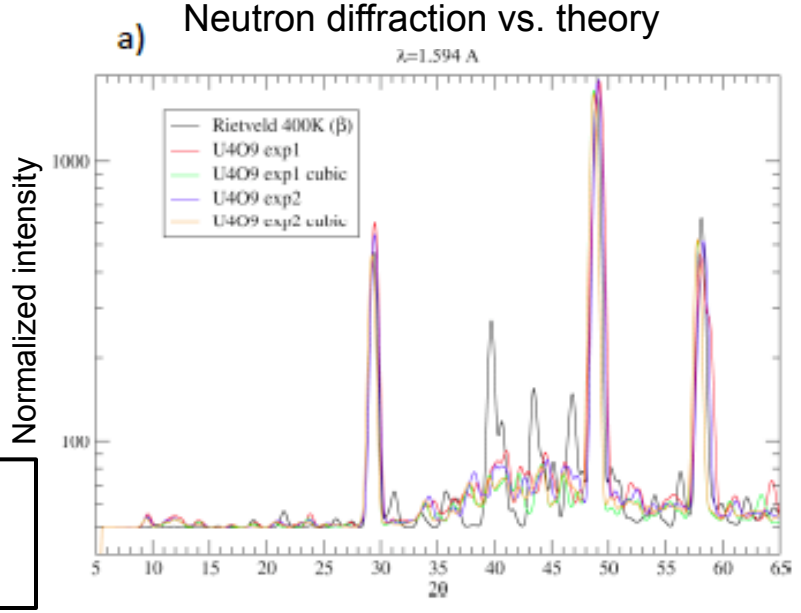

Collaboration with G Baldinozzi (ECP) and L. Desgranges (CEA).

New Model for Low Temperature Phase of U_3O_7 Derived from DFT

U_3O_7

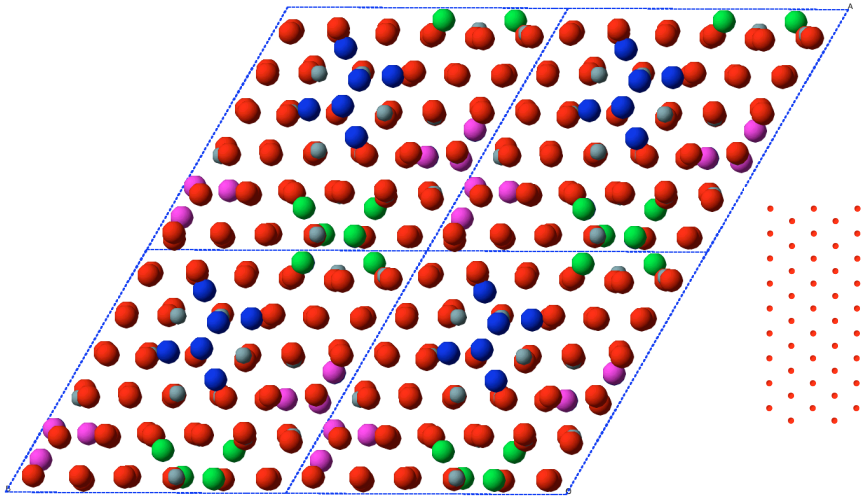

Ordering of oxygen clusters on {111} planes in U_3O_7

UO_2

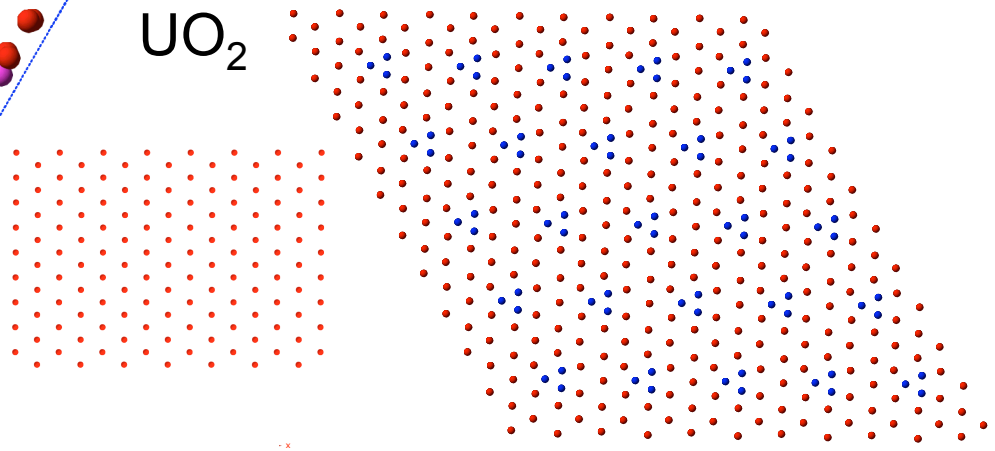

- Compared to U_4O_{9-y} the oxygen clusters are one step closer in each direction. Same ordering rules.
- U_3O_7 is predicted to be exactly stoichimetric.
- Disordering of clusters and U^{5+} ions at finite T lead to polymorphs.
- Due to the complexity of the predicted structures it was not possible to perform optimization, only comparison.

b) Neutron diffraction vs. theory

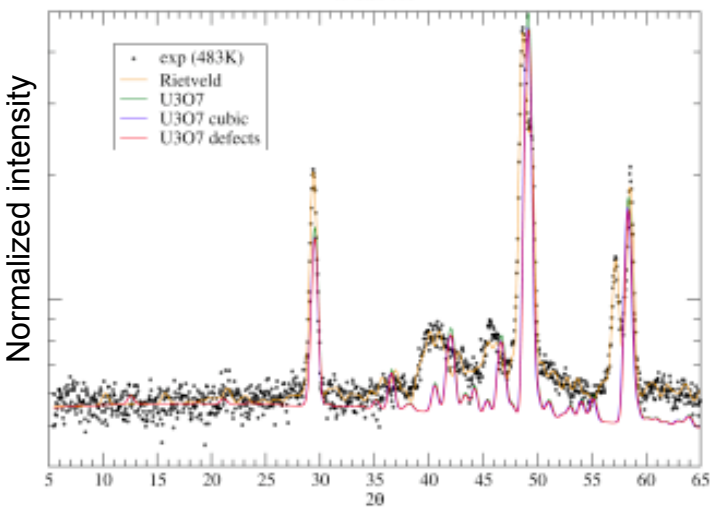

Collaboration with G Baldinozzi (ECP) and L. Desgranges (CEA).

UO_{2+x} (0<x<2/3) Stability Diagram

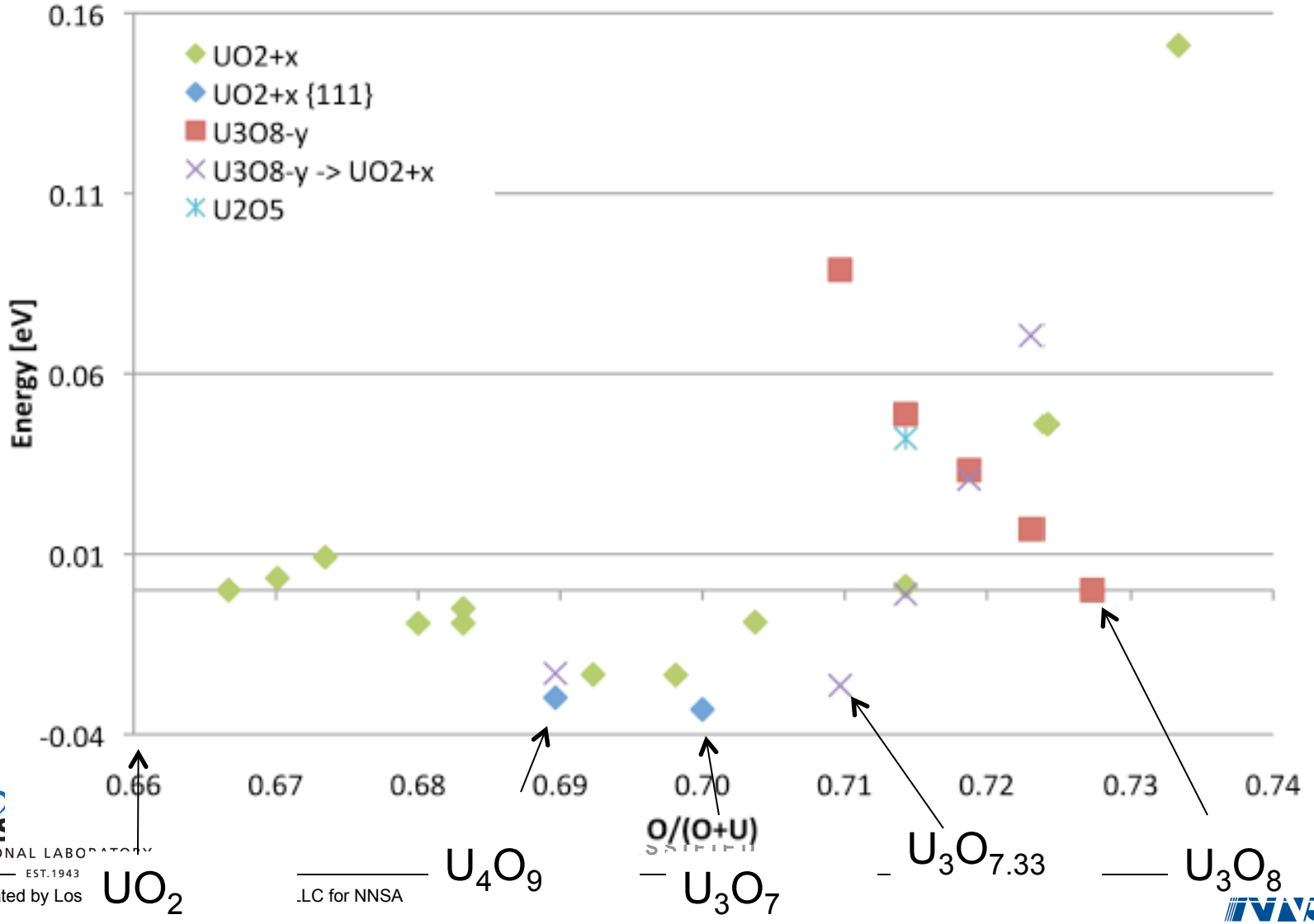

UO_{2+x} (0<x<2/3) Volume Diagram

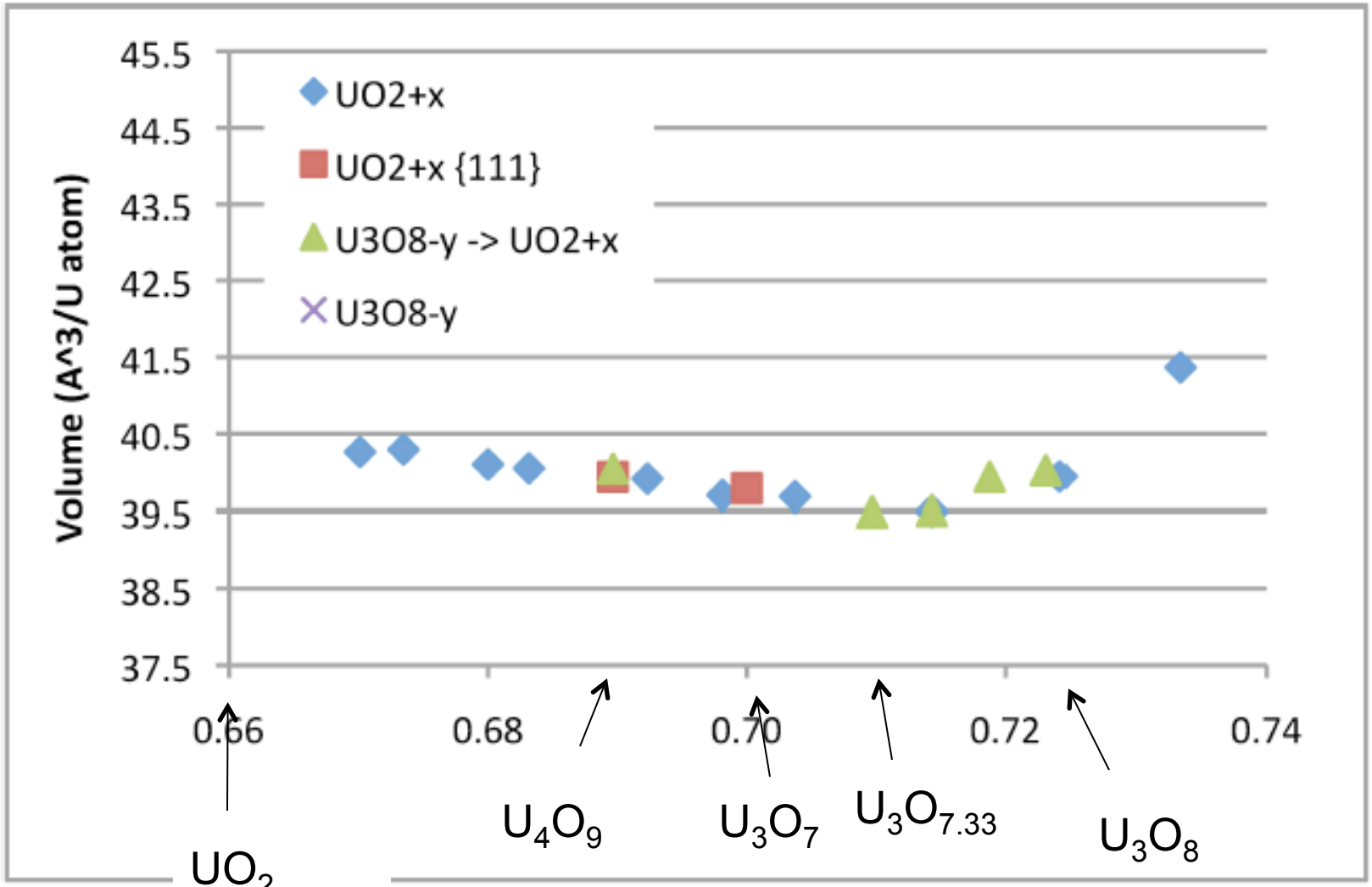

Diffusion of Split Di-interstitials

- Split di-interstitial (I_2^X) can diffuse via intermediate state which is octahedral I_2 structure (I_2^O)
- Migration barrier is 0.47 eV, compared to 0.81 eV for mono-interstitials (interstitialcy mechanism).

Collaboration with C. Deo et al., Georgia Tech.

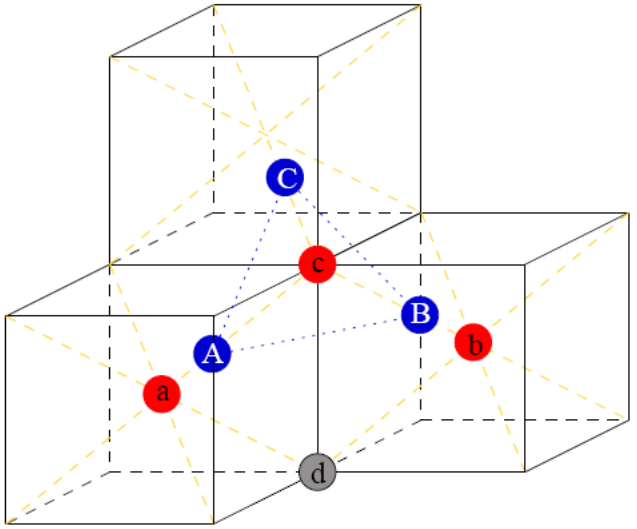

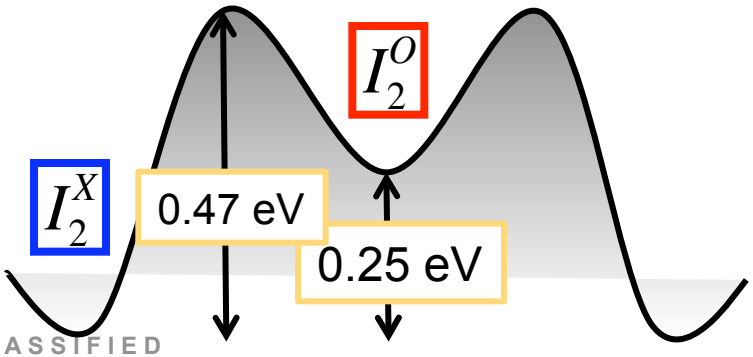

Diffusion of Split Quad-Interstitials

- Split quad-interstitial (I_4^X) can diffuse via one component I_2^X "rotating" to new position
- Migration barrier is 0.97 eV, compared to 0.81 eV for mono-interstitials.

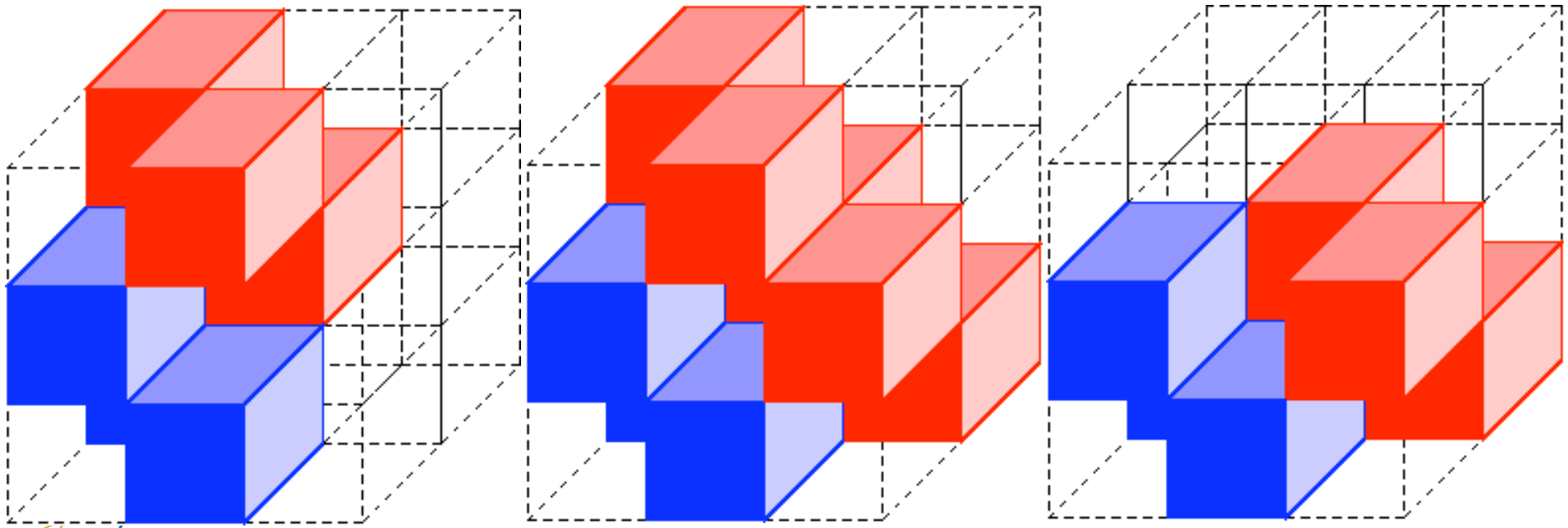

kMC Models for Oxygen Self-Diffusion

Taku Watanabe, Rakesh Behera and Chaitanya Deo

Georgia Institute of Technology

- **Model 1: mono-interstitials only (Murch model)**
  - I_1 diffuse with barrier of 0.81 eV
  - I_1 block all nearest neighbor sites
- **Model 2: mono- plus di-interstitials**
  - Philosophy: as simple an extension of Murch as possible
  - I_1 diffuse with barrier of 0.81 eV
  - I_2 form when 2 I_1 become neighbors
  - I_1 can be neighbors of at most one other I_1 (forming I_2)
    - If an I_1 tries to jump to a site where it would neighbor more than one other I_1, that move is unallowed
  - I_2 diffuse with barrier of 0.47 eV
    - I_2 cannot be nearest neighbor of any other species (like Murch blocking)
  - I_2 are higher in energy than $2*I_1$ by 0.38 eV (from LDA+U)
  - Breakup barrier of I_2 would be 0.43 eV (0.81-0.38)
    - Position of new I_1 would depend on available sites

Diffusion: Theory vs Experiment

- KMC simulation of oxygen self-diffusion in UO_{2+x} at 1073 K
- Results agree well at low x
  - Likely describing mono-interstitial diffusion well
- At larger x, I_1 model quickly falls off, in disagreement with experiment
- By including the split di-interstitial mechanism, we are able to better reproduce the experimental data.
  - Mainly due to different different blocking
- Larger clusters for high x? I_1 or I_2 vs. I_4 barriers agree with conductivity experiments.

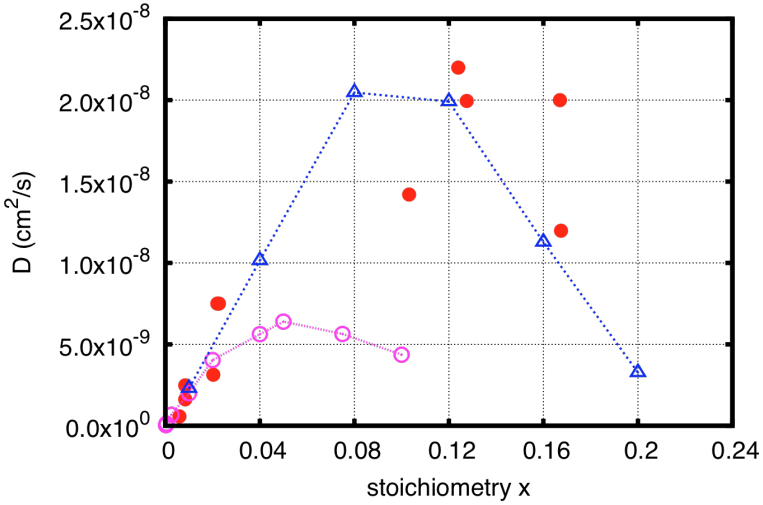

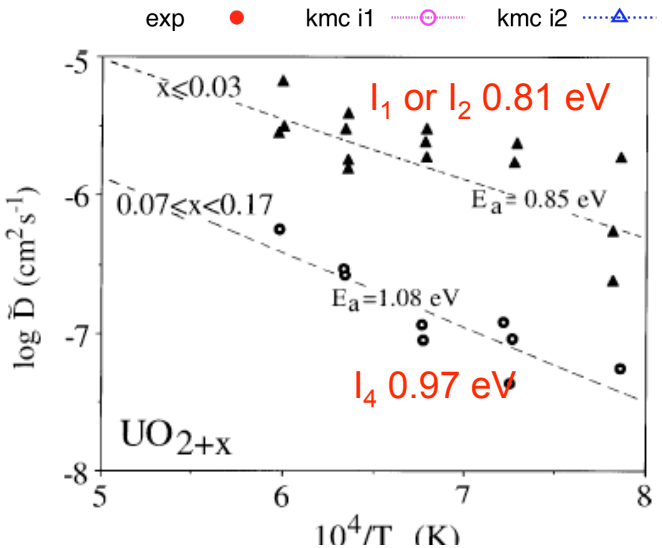

P. Ruello, G. Chirlesan, G. Petot-Ervas, C. Petot, L. Desgranges, Journal of Nuclear Materials **325, 202–209 (2004).**

Improved Description of Cluster Diffusion in UO_{2+x}

Quad-interstitial

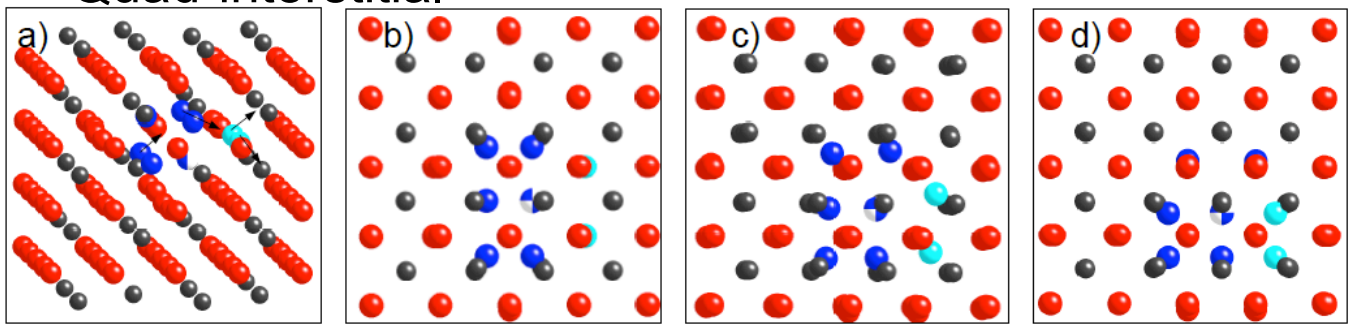

Ruello et al.

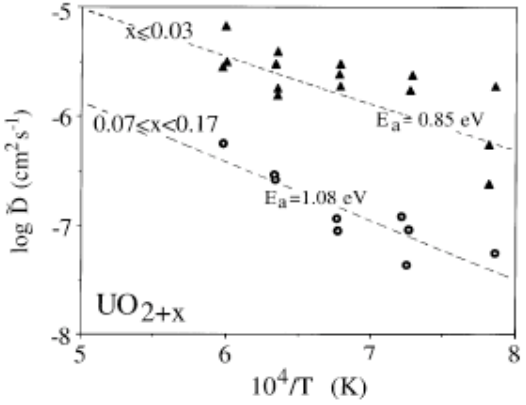

Di-interstitial

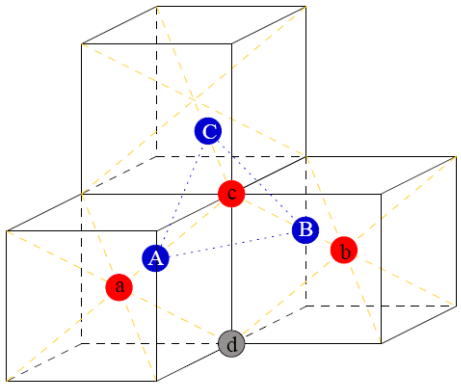

Mono-interstitial (from Dorado et al.)

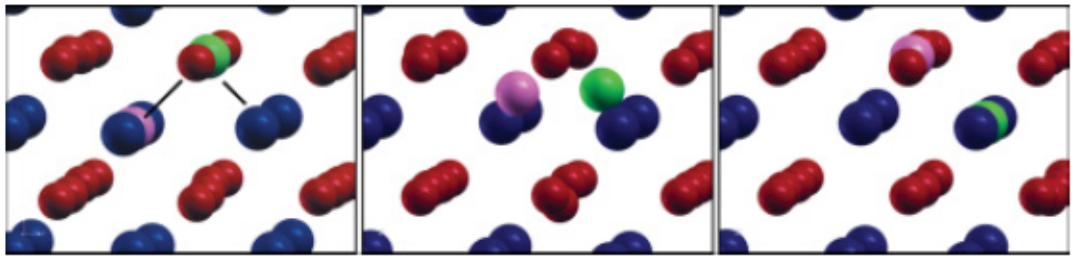

- Exp. barriers: I_1:~1.3 eV, I_2: 0.85 eV, I_4:1.08 eV
- Calculated barriers: I_1:1.31 eV, I_2: 0.87 eV, I_4:1.13 eV
- Implement in kMC for upscaling to continuum.

Summary

- Bulk Xe diffusion in $UO_{2\pm x}$ occurs by binding a second V_U to the Xe trap site clusters.
- Segregation thermodynamics of Xe to different grain boundaries obtained from atomistic simulations and transferred to continuum free energy models suitable for diffusion simulations.
- Effect of grain boundaries and fission gas on thermal conductivity simulated using MD.
- From DFT the split quad-interstitial (I_4^X) emerges as the most stable form of O interstitials in UO_{2+x}.
- With I_4^X as building block the oxidation from fluorite UO_2 via U_4O_9 and U_3O_7 up to U_3O_8 was simulated using DFT.
- Diffusion mechanisms of I_1, I_2 and I_4 clusters established and the calculated migration barriers agree with experiments.